Journal Pre-proofs

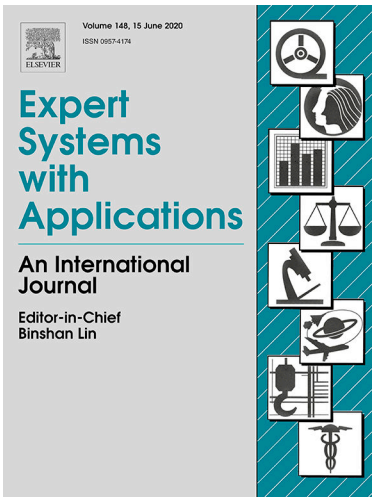

Image completion based on segmentation using neutrosophic sets

Amanna Ghanbari Talouki, Abbas Koochari, S. Ahmad Edalatpanah

PII: S0957-4174(23)02271-6
DOI: https://doi.org/10.1016/j.eswa.2023.121769
Reference: ESWA 121769

To appear in: *Expert Systems with Applications*

Received Date: 11 February 2023
Revised Date: 24 August 2023
Accepted Date: 19 September 2023

Please cite this article as: Ghanbari Talouki, A., Koochari, A., Ahmad Edalatpanah, S., Image completion based on segmentation using neutrosophic sets, *Expert Systems with Applications* (2023), doi: https://doi.org/10.1016/j.eswa.2023.121769

Image Completion based on Segmentation using Neutrosophic Sets

Amanna Ghanbari Talouki[a] , Abbas Koochari[b*] , S. Ahmad Edalatpanah[c]

a. Department of Computer Engineering, Islamic Azad University, Science and Research Branch, Tehran, Iran. amanna.ghanbari@gmail.com, Orcid link: https://orcid.org/0000-0001-5326-4075, Full Address: Science and Research Branch, Daneshgah Blvd, Simon Bolivar Blvd, Tehran, Iran, Postal Code: 1477893855.

b. Department of Computer Engineering, Islamic Azad University, Science and Research Branch, Tehran, Iran. koochari@srbiau.ac.ir, Orcid link: https://orcid.org/0000-0003-0584-6470, Full Address: Science and Research Branch, Daneshgah Blvd, Simon Bolivar Blvd, Tehran, Iran, Postal Code: 1477893855, Tel: 00989373297452.*

c.Department of Applied Mathematics, Ayandegan Institute of Higher Education, Tonekabon, Iran. saedalatpanah@gmail.com. Orcid link: https://orcid.org/0000-0003-0584-6470, Full Address: Ferdowsi St, Tonekabon, Mazandaran Province, Postal Code: 4681853617.

Abstract

Image completion aims to restore the corrupted regions in an image. One of the most important challenges in image completion is to find the most appropriate data for replacing in the hole. In this paper, we proposed a novel image completion method which applies neutrosophic-based segmentation to fill in the hole. Since neutrosophic is useful to interpret indeterminacy included in images, we applied neutrosophic-based image segmentation to decrease spatial and intensity ambiguities exist in images while we have more boundary and homogeneity preservation and less discontinuity. Our exemplar-based image completion algorithm starts from the outer pixel with the maximum priority and iterates until there is not any pixel in target region. Our extended similarity measure considers both neighbourhood and similarity based on results of our innovative neutrosophic-based image segmentation algorithm to find the patches with the maximum match for hole completion. Results show that our approach introduces an improvement of 18% for ASVS (Average Squared Visual Salience) compared to earlier methods. We also gained 0.9919 and 38.96 for MSSIM (Mean of Structure Similarity) and PSNR (Peak Signal to Noise Ratio), respectively while the best values for earlier methods were 0.9868 and 36.75 for MSSIM and PSNR, respectively which is the effect of using neutrosophic segmentation.

Keywords

Image completion; image inpainting; image segmentation; hole filling; neutrosophic sets

1. Introduction

According to essential roles of images in our daily lives and also, advances in computer data collection systems, anybody may gather lots of images; but usually cannot process them manually. Therefore, since representation and digital processing of these kinds of data are possible, image processing becomes attractive. Thanks to fast computers and processors, image processing becomes the most usual processing technique which is used in medical images, remote sensing images, security camera videos and natural image/videos. Image processing performs an essential role in various information access systems to improve the cognition level and facilitate the decision-making process (Sufyan & Badnerkar, 2015).

Image completion is an attractive subject in image processing field which is used for reconstruction of damaged portions of images. The basic goal of image completion was to fill in the damaged regions of an old picture; this is done such a way that restoration does not cause much heterogeneity from the viewer's point of view (Newson et al., 2014). Image completion problems involve a wide range of applications such as protection of historical relics (Ahmed et al., 2021), restoration of old photographs (Quan et al., 2022), biomedicine (Tran et al., 2021), etc.

Image inpainting or image reconstruction are synonyms of image completion. There are some objects in images which may overlap other objects of that or they themselves may be overlapped by some other objects in image; in both cases, removing the overlapped or overlapping object causes a hole in image (Bertalmio et al., 2022).

The major challenging question in image completion is how to find data with maximum match to fill in the corrupted regions while preserving the visual consistency for the resulted image; this question has introduced

various image completion algorithms which some of them focus on different methods of completion and some other ones consider various similarity measures to find the patch with the maximum match (Romero et al., 2022).

Some image completion algorithms benefit image segmentation results to introduce a similarity measure based on the segmented images with the aim of finding the most appropriate patch for filling in the hole and some do not apply segmentation. Image segmentation is applicable for wide usages such as object recognition, robot vision and medical imaging and so on (Guo & Cheng, 2009) and is one of the most challenging tasks in image processing which divides an image into various regions in such a way that each region is itself homogeneous but there is no similarity between two regions.

The world surrounding us include indeterminacy which will be appeared in images and videos of the world. Indeterminacy brings forward ambiguity about components (edges, …) in images which ends to ambiguity in image segmentation. Since image segmentation is used for image completion, it is important to segment the image correctly. Neutrosophic sets consider indeterminacy exists in images and untangle it using three membership functions: truth, indeterminacy and falsity. More accurate segmentation leads to more accurate image completion.

Lack of researches which consider indeterminacy in image completion and also introducing a more pleasant image segmentation which decreases spatial and intensity ambiguities of images and guides us to have segmented images with more boundary and homogeneity preserving in addition to less discontinuity, motivated us to utilize image segmentation using neutrosophic sets and introduce a similarity measure based on the segmented image to find the most appropriate data from undamaged parts of the image to complete the hole in this paper.

Image completion is an expert system which fills in the hole intelligently. The system which applies our proposed algorithm begins from where has the biggest gradient and systematically finds the most appropriate data for replacing in the hole. This system benefits a knowledge base and an inference engine; the knowledge base is the source region (those parts of image that are not corrupted) and inference engine is the proposed algorithm which searches knowledge base using a similarity measure aiming to find the best patch for hole filling.

Note that some problems such as pixel classification, inherent weaknesses of the acquisition and the imaging mechanism, the quantization noise and nonlinear behaviour of the mapping system result in introducing indeterminacy in images (Salama et al, 2014). Irvanizam et al. (2022) applies trapezoidal fuzzy neutrosophic numbers to overcome weaknesses in group decision making. Two other researches proposed by Song et al. (2020) and Irvanziam et al. (2021) solve group decision making problems by managing noises in images using combination of saliency map and neutrosophic sets, and bipolar neutrosophic sets, respectively.

2. Related Works

Human beings benefit image processing for various purposes such as expressing and transmission of information which nowadays are very useful and important for daily lives according to fast processors and various imaging systems which bring out lots of available images. Yet, information storage and transmission always confront losses and it is inevitable for images. Also, images may be corrupted because overlapping occurs in images when some unwanted objects exist in image; removing these overlapping brings out holes in images (Li & Chen, 2022). Fig. 1 shows damages made in image which image completion aims to recover them.

(a) (b)

Fig. 1: Recovering a damaged image using image completion method (Ghanbari Talouki & Soryani, 2011). (a) Damaged image (b) Recovered image

Fig. 2 illustrates hole caused by an overlapping object which image completion aims to fill in that. As it is obvious in Fig. 1 and Fig. 2, image completion means setting appropriate values for pixels placed in missing region. Researchers investigate various techniques to find these valid values. Image completion techniques can be divided into two major categories: 1) Techniques which do not need training. 2) Techniques which need training. The former category is named traditional methods and the later one is named machine learning methods.

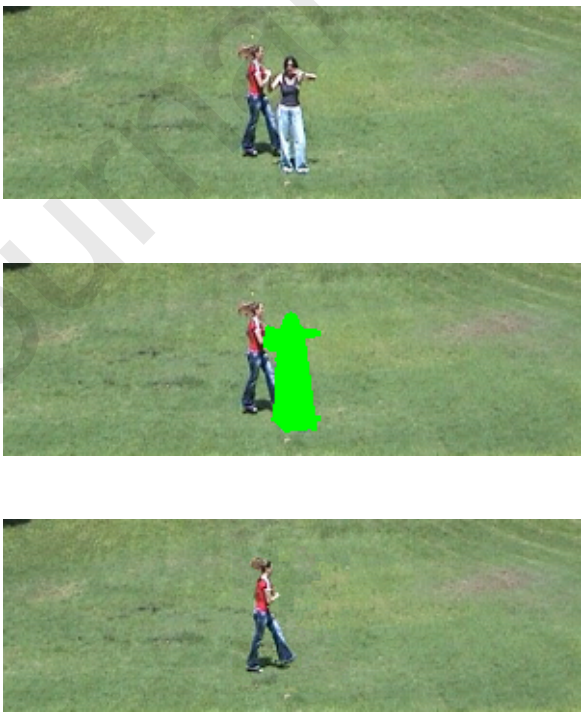

(a)

(b)

(c)

Fig. 2: Hole Completion. (a) Original image (Ghanbari Talouki & Majdi, 2019) (b) Hole caused by an overlapping object which is shown in green. (c) Result of image completion

2.1. Traditional image inpainting techniques

Traditional methods are composed of exemplar-based and diffusion-based techniques. Exemplar-based techniques are also consisted of pixel-based and patch-based methods.

Patch-based methods are widely used and present more qualified results (Ghanbari Talouki et al., 2017). Jia et al. (2006) and Ding et al. (2007) are examples of researches which apply patch-based methods for image completion.

In patch-based methods, information needed for filling in the missing region of damaged images are obtained using intact patches from different parts of image. In diffusion-based methods, missing region is filled by diffusing the surrounding pixels from the boundary (Cherel et al., 2022).

2.1.1. Patch-based methods

Patch-based methods are group of methods which consider the uncorrupted parts of image and choose patches from them with the aim of filling in the hole. As it is obvious, it is very important to preserve similarity for the selected patch. Different algorithms apply different methods to introduce an admissible similarity measure which helps to get to the purpose of preserving the similarity of the selected patch to the target region which is missed and is going to be completed (Ling et al., 2011). Patch-based methods propose satisfactory results; yet, they depend on existence of missing information in somewhere in undamaged parts of the image. Furthermore, finding an appropriate patch which brings out admissible similarity needs abundant searching and comparing, so it takes long time, therefore patch-based methods are very time consuming. Formerly discussion leads to introducing novel approaches which propose more applicable similarity measures to find acceptable patches. Zhou et al. (2016) proposed a coherent direction-aware patch alignment approach which brought out an acceleration in patch searching and introduced patches with more similarity in patch matching phase. This research also benefits less time consuming compared to earlier methods. Cho et al. (2022) introduced a context-aware image completion algorithm which was based on patches and applied textural descriptors to find patches with the maximum match. Context-aware algorithm means they used different size of blocks for dividing the image regarded to context of the image. They exerted Markov random field to encode other neighbourhood patches' priori knowledge. Texton histogram which is used to find the interior texture of a local region proposed the contextual descriptors. Jayachandran and Dhanasekaran (2013) utilized nearest neighbour matching approximation to speed up finding the best match and overcome lack of efficiency which is disadvantage of patch-based techniques because of their time consuming and exhaustive searches for finding a valid patch. Fig. 2 shows an example of patch-based method.

2.1.2. Diffusion-based methods

Diffusion-based techniques essentially complete target regions by diffusing neighbouring pixel information. They apply partial differential equations. There are some disadvantages for these algorithms for exampleartifacts appear as local variance difference and noise pattern, when completion is done (Dou et al., 2020). A diffusion-based approach was proposed by Prasath et al. (2014) which is useful for limited dataset and operates on lower structures of texture and geometric constructions. There are limitations for this method: it only considers small-scale images. If the missing region is large or there are complex structures in damaged image, results will show inconsistency for structure and texture and plague some artifacts in recovered image. Fig. 3 depicts an example of diffusion-based image completion.

(a) (b)

Fig. 3: diffusion-based image completion (Li et al., 2017) (a) Corrupted image; black region is the missing region. (b) Result of image completion; region inside of the dashed line is restored.

2.2. Machine learning image completion techniques

Deep learning approaches are able to produce acceptable results for complex scene, therefore they are used for image completion. They benefit large-scale datasets which make training possible.

2.2.1. CNN-based methods

Convolution Neural Network structures provide some special architectures for image completion applications. The U-Net architecture which was used in Shift-Net image completion (Yan et al., 2018) receive an image and a mask of missing region, then put them into convolutional layers. General structure of image in addition to its fine details. Fig. 4 shows U-Net architecture and Fig. 5 shows shift-Net architecture which is U-Net with specific shift connections.

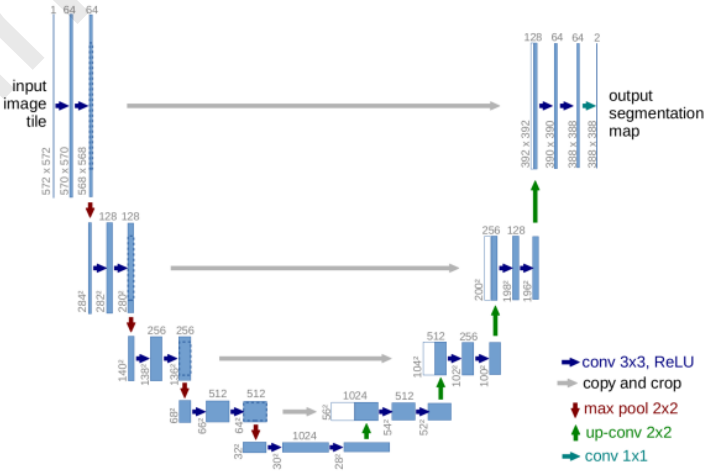

Fig. 4: U-Net architecture (Yan et al., 2018)

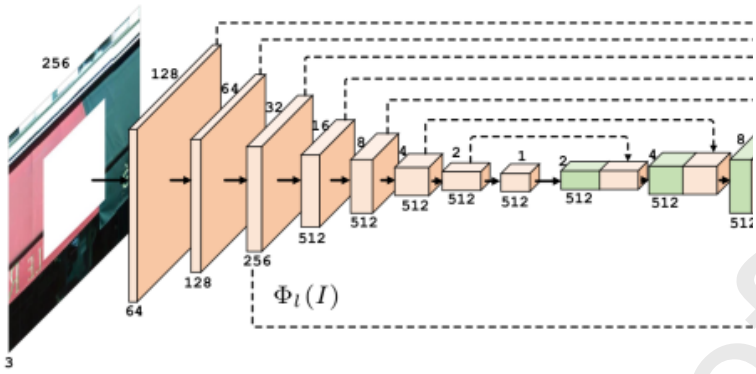

Fig. 5: Shift-Net architecture (Yan et al., 2018)

2.2.2. GAN-based methods

GAN-based methods provide realistic results. Jo and Park (2018) applied GAN-based systems to complete masked image with the use of given sketch. Fig. 6 illustrates a model with dilated convolution layer.

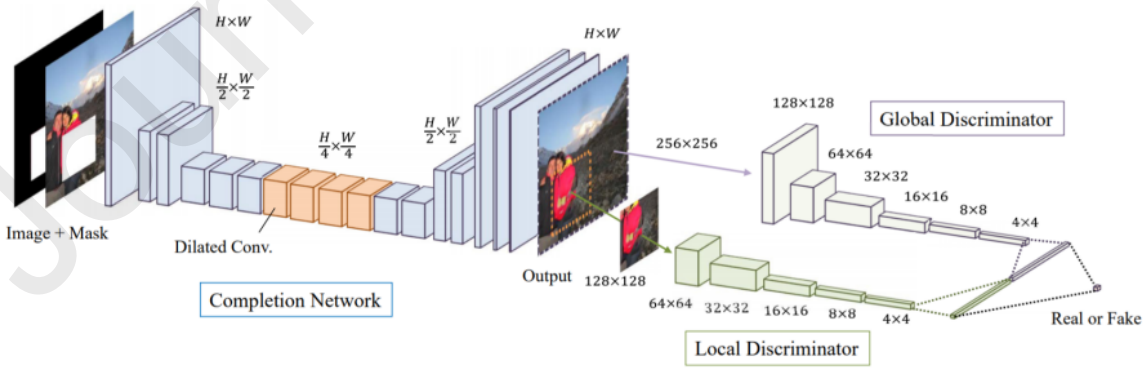

Fig. 6: Model with dilated convolution layer (Jo & Park, 2018)

3. Proposed Method

Here, we describe the proposed method in details. To begin with, we firstly state the concept of digital image as a math problem. In the following, we ingeminate the exemplar-based image completion method which had been initially introduced by Criminisi et al. (2004) and then was used for different purposes in many researches (Zhang et al., 2019; Shajahan et al., 2019; Shroff et al., 2019; Mousavi et al., 2022; Li et al., 2022; Zhao et al., 2022). As mentioned earlier, we apply image segmentation in our research and complete the hole in images by the help of extended exemplar-based image completion which considers the result of segmentation to find the most suitable patch for filling in the hole. Therefore, we explain neutrosophic sets-based image segmentation which is efficient because it considers indeterminacy. Next we describe our novel image completion method which introduces similarity measure based on results of image segmentation.

3.1. Digital Image Definition

A digital image is defined as Eq. (1):

$$P = \{[x,y]^T | x,y \in \mathbb{N}, 1 \le x \le w, 1 \le y \le h\} \quad (1)$$

Where P is all of the points included in an image of size $w \times h$ (w is the width and h is the height). x and y are coordinates which identify a special pixel. $p = [x,y]^T$ shows each pixel, individually; so, we have:

$$I{:}P \rightarrow [0,255]^d \subset \mathbb{Z}^d$$

I is the image, set d=1 for grayscale images and d=3 for color images. p is the pixel and I(p) is the light intensity of image at pixel p for gray scale images and is color of pixel p for color images (Ghanbari Talouki et al., 2021).

3.2. Exemplar-based Image Inpainting algorithm

Exemplar-based image inpainting algorithm which had been initially introduced by Criminisi et al. (2004), is depicted in Fig. 7.

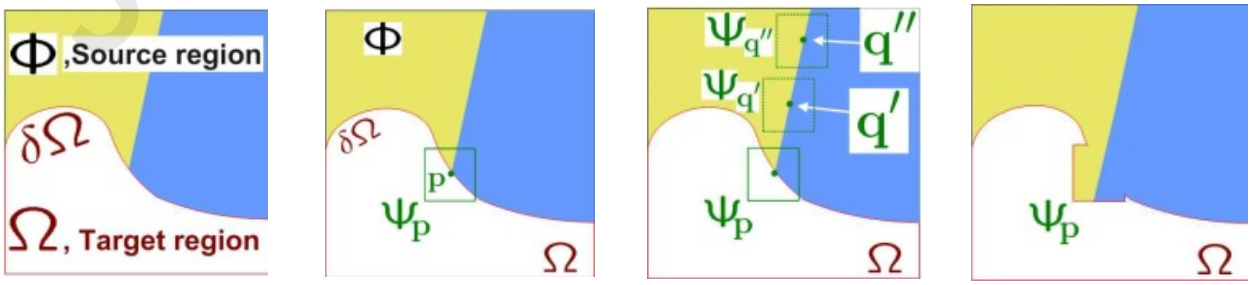

(a) (b) (c) (d)

Fig.7. regions and parameters in Criminisi's exemplar-based image inpainting algorithm (Criminisi et al., 2004). (a) name of different regions. (b) p is the pixel with the highest priority. (c) different patches ($\Psi_{q'}$, $\Psi_{q''}$) are searched in order to find the best match. (d) the best matched patch ever found is placed at Ψ_p

Image completion can be considered as a function of an image *I* and a set of points which are located in the hole and are going to be completed. This function's output *I′* is an image with the same dimensions as the input image where new values are placed instead of the hole. Hole is also known as the "target region" and we will display it by ΩCP. While image completion continues, target region gradually gets smaller and smaller so that finally, no pixel belongs to this region. Eq. (2) states the completion function which is shown by *C*:

$$I'=C(I,\Omega) \quad (2)$$

Border of Ω is a set of pixels in Ω which at least one of the neighbouring pixels of them is not a member of Ω. This collection points are displayed as $\delta\Omega$.

To complete the hole existed in an image, Criminisi et al. (2004) uses information included in the non-damaged parts of that image. This area that has the correct information, is named by the reference region or the source region. Source region is displayed as Eq. (3):

$$\phi = P - \Omega^0 \quad (3)$$

Where Ω^0 shows the damaged region when the completion algorithm starts. As mentioned before, the hole changes by algorithm iteration. Consequently, we mention to the hole at the first step by Ω^0 and at the current step by Ω^t to distinguish between them; yet, when it is clear, Ω is used generally.

In the following, a priority value is defined for each individual pixel placed on the boundary of the corrupted region by Eq. (4); this priority value specifies which pixel firstly must be considered to be completed. The pixel with the highest priority wins to define patch Ψ_p.

$$pr(p) = Cn(p)Dt(p) \quad (4)$$

Where $Cn(p)$ and $Dt(p)$ are confidence and data values, respectively which are defined by Eq. (5) and (6).

$$Cn(p) = \frac{\sum_{q \in \Psi_p \cap (I-\Omega)} Cn(q)}{|\Psi_p|} \quad (5)$$

$$Dt(p) = \frac{|\nabla I_p^{\perp} . n_p|}{\gamma} \quad (6)$$

Where $\boldsymbol{\Psi p}$ shows a patch centered at pixel $\boldsymbol{p}$ which its area is $|\boldsymbol{\Psi p}|$. $\boldsymbol{\gamma}$ is a normalization factor ($\boldsymbol{\gamma}$ =**255** for greyscale images). $\boldsymbol{n_p}$ is the orthogonal unit vector to the boundary of the hole and $\perp$ shows the orthogonal operator. The confidence term $Cn(p)$ specifies the amount of reliable information exists around the pixel p.It is clear that we aim to complete first those pixels which have more reliable information; these information may be included in the image because of two reasons: 1) The surrounded pixels are placed in the source region. 2) The surrounded pixels were completed before. Initial value for $Cn(p)$ is 0 for pixels of the target region and 1 for pixels of the source region. $Dt(p)$ shows the strength of isophotes which hit the front $\delta\Omega$ at each iteration. Data term is important because it makes linear structures to be synthesized first, and, therefore propagated securely into the target region. Fig. 8 shows parameters used in Eq. (6) to find data term for pixel p.

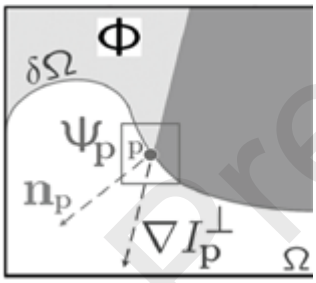

Fig. 8: parameters used in Eq. (6) to find data term for pixel p

Consider the patch with the highest priority is $\boldsymbol{\Psi p'}$ and the patch $\boldsymbol{\Psi q'}$ is the best match of $\boldsymbol{\Psi p'}$ found in the source region. In order to replace $\boldsymbol{\Psi p'}$ with $\boldsymbol{\Psi q'}$, only those pixels of $\boldsymbol{\Psi p'}$ which are in the target region, will obtain new values. Now, the confidence value of pixels surrounded the remaining portion of the hole are updated.

This process iterates until the target region is completed. The exemplar-based method preserves both structure and texture and therefore, is suitable for background inpainting.

If the occluding object is static, this completed hole is copied into other frames. Yet, considering a moving object, there is no need for inpainting; information about the region behind the moving occluding object can be used for filling in hole.

This algorithm finds priority of all pixels of $\delta\Omega$. Then, the patch $\boldsymbol{\Psi p'}$ with the highest priority value for pixel p is selected. Source region is searched to find the best match for $\boldsymbol{\Psi p'}$ using Eq. (7):

$$\arg\min_{\boldsymbol{\Psi_q} \in \Phi} d(\boldsymbol{\Psi}_p, \boldsymbol{\Psi}_q) = \boldsymbol{\Psi}_q \quad (7)$$

Where $d(\Psi_p, \Psi_q)$ is the sum of squared differences (SSD) of intensities of two patches Ψ_p and Ψ_q.

Once we found the best match patch Ψ_q, those pixels of Ψ_p which are in the target region, will be replaced by the corresponding pixel values of Ψ_q. Then, confidence value for pixels belonging to the boundary of Ψ_p which they intersect with the target region, are updated using Eq. (8):

$$C(p) = C(p') \quad \forall p \in \Psi_p \cap \Omega \tag{8}$$

It iterates until there is no pixel in the target region which means the hole is fully completed.

3.3. Image segmentation

Segmentation procedure receives an image and gives a set of regions S_i which satisfy these clauses (Chen et al., 2022):

I. $\cup S_i = S$; Each S_i is a particular partition which shows a segment. Union of these particular partitions leads to the reference image S.
II. $S_i \cap S_j = \emptyset, i \neq j$; Regions do not have any intersection. Two regions introduce two different segments while there is no intersection between them.
III. $\forall S_i, P(S_i) = true$; Homogeneity predicate is satisfied for each region.
IV. $P(S_i \cup S_j) = false, i \neq j, S_i\ adjacent\ S_j$; Homogeneity predicate is not satisfied for union of adjacent regions.

The above four clauses guarantees an original image is divided into some distinct segments which there is not any intersection between them; yet, each particular segment is homogenous itself. As a result, we can handle each segment, distinctly.

Image segmentation is a crucial step in image processing applications. There are some matters which affect image segmentation's results: intensity, texture, contrast, blurring, noise and number of clusters; these features affect the quality and accuracy of the output of segmentation. Image segmentation aims to extract all of the meaningful objects existed in image; yet, it is difficult to omit human interaction when segmentation is in process (Luo et al., 2022).

3.3.1. Neutrosophic sets

Neutrosophic was firstly introduced by Smrandache (1998). There are three concepts which are considered by neutrosophic sets: indeterminacy, membership and non-membership functions. A neutrosophic set A in U is as u(T,I,F) where three values T_A(u), I_A(u) and F_A(u) are subsets which respectively show truth, indeterminacy and falsity membership functions and the values are standard or non-standard real numbers in [0,1].

$T_A: U \rightarrow [-0\ ,1+]$

$I_A: U \rightarrow [-0\ ,1+]$

$F_A: U \rightarrow [-0\ ,1+]$

Where we have the following constraint for summation of T_A(u), I_A(u) and F_A(u):

$$0 \leq sup\ T_A(u) + sup\ I_A(u) + sup\ F_A(u) \leq 3$$

Where sup is the abbreviator of suprimum. As described earlier, each of three subsets T_A(u), I_A(u) and F_A(u) may be valued by the range of $[-0\ ,1+]$ and sup relates to suprimum value of each of them.

Some researches apply neutrosophic offsets for image segmentation and noise reduction; neutrosophic offsets are neutrosophic sets which their truth values lie outside the interval [0,1] (Smarandache et al. (2020)); yet, some other researches (Hu & Fan (2017)) apply the predefined neutrosophic sets for foreground/background subtraction.

3.3.2. Threshold-based algorithm

Here, neutrosophic sets are applied in partnership with a histogram-based thresholding approach to segment an image. Histogram-based thresholding technique aims to partition an image into some regions considering gray values of that image. Fig. 9 shows the flowchart of the proposed approach.

$h_1,h_2,h_3,...,h_K$ are histogram of pixel values and maximum pixel value is shown by K (K is usually 255). h_l defines number of pixels having gray level l in an image. Threshold-based segmentation approaches find proper thresholds and segment the image using them; neutrosophic sets help to find these admissible thresholds, as a result, to begin with, we map the image into neutrosophic sets using Eq. (9) – (13): (Xu et al., 2018)

$$t(i,j) = \frac{\overline{g(i,j)} - \overline{g_{min}}}{\overline{g_{max}} - \overline{g_{min}}} \tag{9}$$

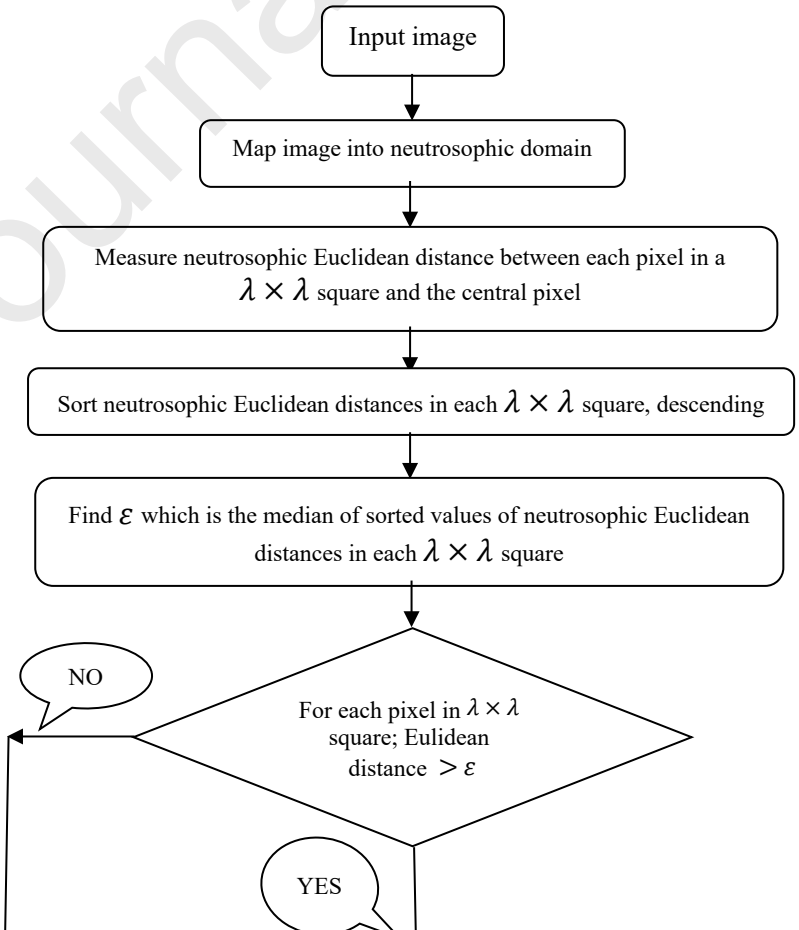

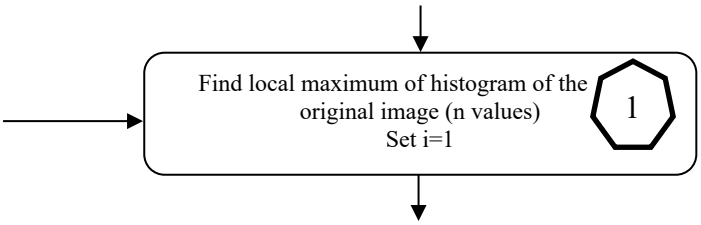

Fig 9: Schematic diagram of the proposed method (continued)

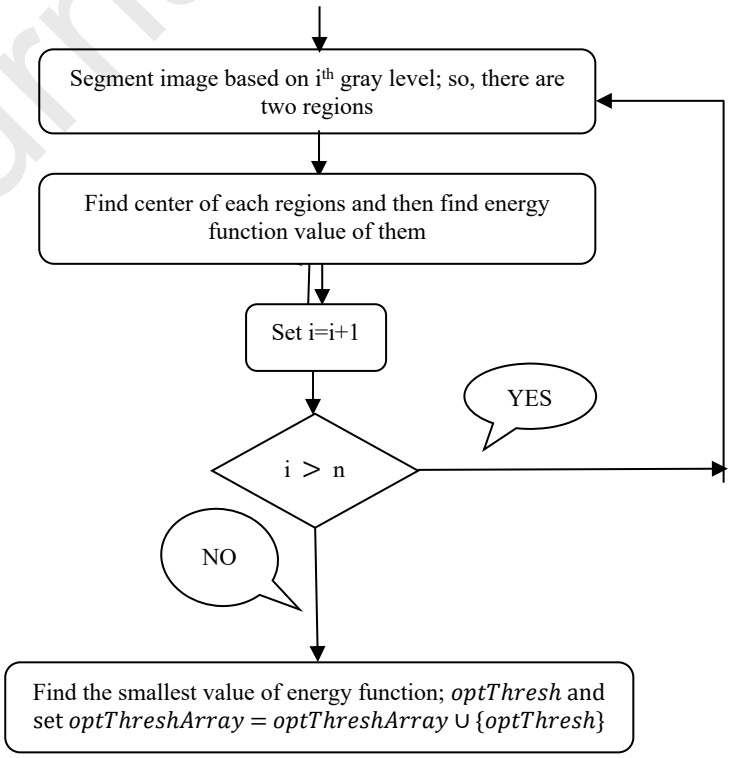

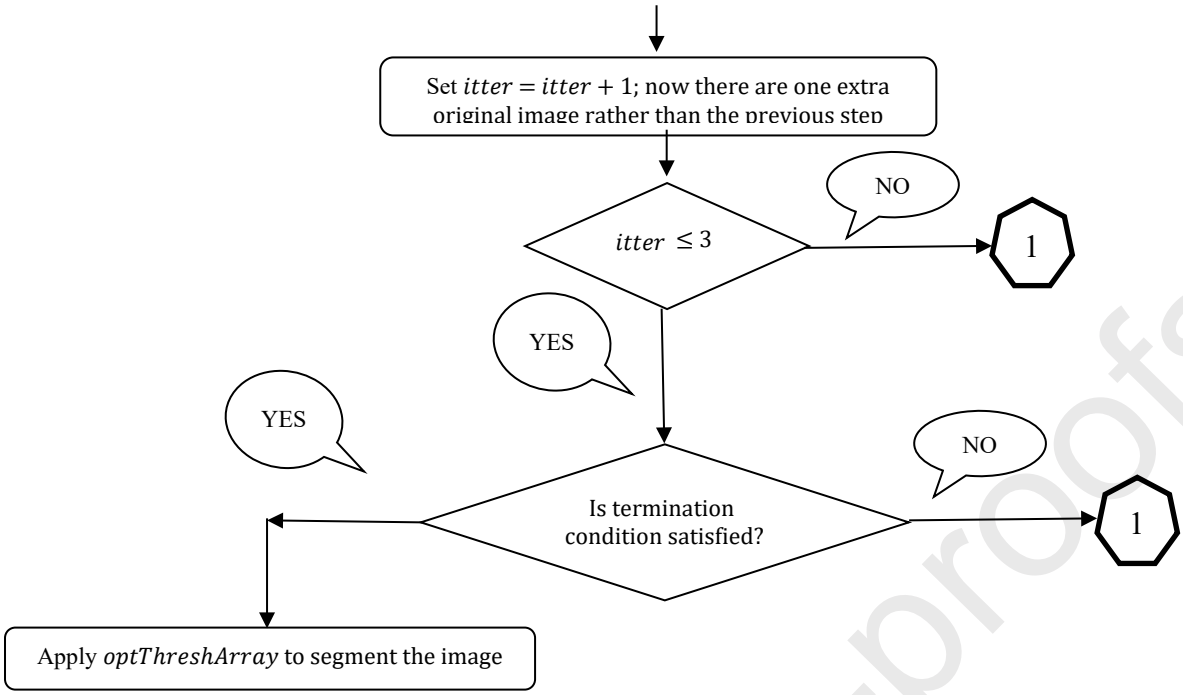

Fig 9: Schematic diagram of the proposed method

$$i(i,j) = \frac{\delta(i,j) - \delta_{min}}{\delta_{max} - \delta_{min}} \tag{10}$$

$$f(i,j) = 3 - t(i,j) - i(i,j) \tag{11}$$

$$\overline{g(i,j)} = \frac{1}{w \times w} \sum_{m=i-w/2}^{i+w/2} \sum_{n=j-w/2}^{j+w/2} g(m,n) \tag{12}$$

$$\delta(i,j) = abs\big(g(i,j) - \overline{g(i,j)}\big) \quad (13)$$

Where t, i and f stand for truth, indeterminacy and falsity membership functions, respectively. $g(i,j)$ shows intensity of pixel $p(i,j)$ and $\overline{g(i,j)}$ is mean of pixel intensities for those pixels placed inside a $w \times w$ window; this $w \times w$ window rolls over top left of the image into bottom right in order to cover all pixels of the image. g_{max} and g_{min} are maximum and minimum values of all $\overline{g(i,j)}$ for the whole image, respectively. $\delta(i,j)$ is the absolute difference between $g(i,j)$ and $\overline{g(i,j)}$. δ_{max} and δ_{min} are maximum and minimum of $\delta(i,j)$ for all pixels, respectively. The given image img_{NS} is the previous image but in neutrosophic domain which means each pixel in img_{NS} has three values obtained from Eq. (9) – (13).

In the following, we group similar pixels in image img_{NS}. We determine neighbourhood in which pixel similarities in image img_{NS} is measured, by a square of size $\lambda \times \lambda$ where λ is an integer number. In this study, we set $\lambda = 7$. Comparison point is the pixel which is placed at the center of this $\lambda \times \lambda$ square. We measure Euclidean distances between the former mentioned comparison point and the remaining pixels in $\lambda \times \lambda$ square by Eq. (14) (Ye, 2014).

$$dist_2(A,B) = \left\{\frac{1}{3}|T_A - T_B|^2 + |I_A - I_B|^2 + |F_A - F_B|^2\right\}^{\frac{1}{2}} \quad (14)$$

Where $dist_2(A,B)$ is the Euclidean distance for two points $A(T_A,I_A,F_A)$ and $B(T_B,I_B,F_B)$ in neutrosophic domain; two distinct pixels in $\lambda \times \lambda$ square in img_{NS} are considered as two points $A(T_A,I_A,F_A)$ and $B(T_B,I_B,F_B)$.

Preposition:

A distance measure like $dist_2(A,B)$ with consideration of having three neutrosophic points $A(T_A,I_A,F_A)$, $B(T_B,I_B,F_B)$ and $C(T_C,I_C,F_C)$ preserve four constraints:

i. $0 \le dist_2(A,B) \le 1$

ii. $dist_2(A,B) = 1 \; iff \; A = B$

iii. $dist_2(A,B) = d_2(B,A)$

iv. $if \; A \subseteq B \subseteq C, then \; dist_2(A,C) \ge dist_2(A,B) \; and \; dist_2(A,C) \ge dist_2(B,C)$

Proof. It is obvious that constraints (i) to (iii) are satisfied for Eq. (14). According to constraint (iv), we suppose $A \subseteq B \subseteq C$, therefore, $T_A \le T_B \le T_C$, $I_A \ge I_B \ge I_C$ and $F_A \ge F_B \ge F_C$ and we have following relations:

$$|T_A - T_B|^2 \le |T_A - T_C|^2, |T_B - T_C|^2 \le |T_A - T_C|^2,$$

$$|I_A - I_B|^2 \leq |I_A - I_C|^2, |I_B - I_C|^2 \leq |I_A - I_C|^2,$$

$$|F_A - F_B|^2 \leq |F_A - F_C|^2, |F_B - F_C|^2 \leq |F_A - F_C|^2.$$

Hence,

$$|T_A - T_B|^2 + |I_A - I_B|^2 + |F_A - F_B|^2 \leq |T_A - T_C|^2 + |I_A - I_C|^2 + |F_A - F_C|^2,$$

$$|T_B - T_C|^2 + |I_B - I_C|^2 + |F_B - F_C|^2 \leq |T_A - T_C|^2 + |I_A - I_C|^2 + |F_A - F_C|^2,$$

Combination of the above inequalities and Eq. (14) leads to $dist_2(A,C) \geq dist_2(A, B)$ and $dist_2(A,C) \geq dist_2(B,C)$; constraint (iv) is satisfied and proof is done.

We suppose ε is a decision point; scilicet, distances smaller than ε refer to pixels which are nearly similar. Hence, we can intersect these pixels and assign the obtained intersection value as new value for contributed pixels.

It should be mentioned that in the case of existing more than one analogous pixel to the comparison point of the $\lambda \times \lambda$ square in img_{NS}, in other words, when the distance value for those pixels are smaller than ε (ε is explained later), we mark these pixels. When the $\lambda \times \lambda$ square in img_{NS} is checked, we obtain intersection value for pixels which were formerly marked. It must be noticed that as we mentioned previously, these computation perform on neutrosophic image. Eq. (15) introduces intersection for two neutrosophic sets:

$$C = A \cap B = \{\min(T_A,T_B), \max(I_A,I_B), \max(F_A,F_B)\} \quad (15)$$

Where A and B show two neutrosophic sets and C determine intersection of those sets. We set $A(T_A,I_A,F_A)$ and $B(T_B,I_B,F_B)$ as two distinct marked pixels specified from $\lambda \times \lambda$ square in img_{NS}. The recent truth value is obtained by finding minimum value of truth for neutrosophic sets A and B. The recent indeterminacy value is obtained by finding maximum value of indeterminacy for neutrosophic sets A and B. The recent falsity value is obtained by finding maximum value of falsity for neutrosophic sets A and B. Intersection is given for all marked pixels in a $\lambda \times \lambda$ square. This procedure repeats for the next $\lambda \times \lambda$ square in img_{NS}; it continues until the image is totally checked. Finally we have a new image named img_{NI} which similar pixels receive equal neutrosophic value in recent image.

As we formerly described, ε is a parameter which is used for controlling the similarity; as a result, its influence on the resulted img_{NI} is inevitable. Score function, accuracy and certainty which are separately given for each pixel in $\lambda \times \lambda$ square in img_{NI} help us to find a more reasonable value for ε. Score function, accuracy and certainty are obtained using Eq. (16) to (18), respectively (Broumi et al., 2018):

$$s(A) = \frac{2 + T_A - I_A - F_A}{3} \quad (16)$$

$$a(A) = T_A - F_A \tag{17}$$

$$c(A) = T_A \tag{18}$$

Where $s(A)$ defines score function for a neutrosophic point $A(T_A,I_A,F_A)$, $a(A)$ shows accuracy for a neutrosophic point $A(T_A,I_A,F_A)$ and $c(A)$ shows certainty for a neutrosophic point $A(T_A,I_A,F_A)$.

Next, all pixels within a $\lambda \times \lambda$ square in img_{NI} are sorted ascending according to score function, accuracy and certainty. Further conditions are used to sort neutrosophic values:

i. If $s(A_1) > s(A_2)$, then A_1 is greater than A_2, denoted by $A_1 > A_2$.

ii. If $s(A_1) = s(A_2)$ and $a(A_1) > a(A_2)$, then A_1 is greater than A_2, denoted by $A_1 > A_2$.

iii. If $s(A_1) = s(A_2)$, $a(A_1) = a(A_2)$ and $c(A_1) > c(A_2)$, then A_1 is greater than A_2, denoted by $A_1 > A_2$.

iv. If $s(A_1) = s(A_2)$, $a(A_1) = a(A_2)$ and $c(A_1) = c(A_2)$, then A_1 is equal to A_2, denoted by $A_1 = A_2$.

Where $A_1(T_A,I_A,F_A)$ and $A_2(T_A,I_A,F_A)$ determine two distinct neutrosophic points.

Now we have neutrosophic points in $\lambda \times \lambda$ square in img_{NS} sorted; so, we introduce optimal point to be median of these sorted values. Then, ε is given by obtaining distance between the comparison point and this optimal point. Euclidean distance which was formerly defined in Eq. (14) is used to introduce ε.

The former procedure which is described for one $\lambda \times \lambda$ square, repeats for the whole image and img_{NI} is generated. img_{NI} and the original image, together are used for image segmentation. We select some intensity values as thresholds which are applied to segment the image. In order to have an accurate segmented image, we focus on finding more precise thresholds; thus, we propose our novel algorithm to determine thresholds.

To begin with, we define histogram of the original image img shown by $hist_{img}$ for the first iteration ($itter = 1$). Then, local maximum of $hist_{img}$ which are referred to as $hist_{max}(g_1)$, $hist_{max}(g_2)$, ... ,$hist_{max}(g_k)$,....,$hist_{max}(g_n)$ are determined where $hist_{max}(g_k)$ corresponds to gray level g_k. Next, having a descending sorted list of these local maximum values (note that sorting is done according to pixel counts), we carry the following procedure out from the maximum value into the minimum value of the list.

We name current local maximum which we are working on, as num, also we name intensity value related to num as $thresh$; $thresh$ is the threshold which is used for segmentation. Now, there are two distinct regions R_1 and R_2 according this threshold $thresh$; $R_1 = [minIntensity...thresh]$ and $+1...thresh = [R_2$ $maxIntensity]$ where $minIntensity$ is the minimum intensity included in image (it is generally zero) and $maxIntensity$ is the maximum intensity included in image (it is generally 255). As mentioned earlier, we have two distinct regions R_1 and R_2; we apply Eq. (19) to determine center of R_1 and R_2, separately:

$$c(R_i) = \frac{\sum_{p \in R_i} t(p_{NI}).I(p)}{\sum_{p \in R_i} t(p_{NI})} \tag{19}$$

Where $c(R_i)$ shows the center of region R_i, $t(p_{NI})$ sets truth for pixel p in image img_{NI} and $I(p)$ determines intensity value at pixel p in original image img. Energy function for this current segmentation is (Eq. (20)):

$$E_{NI} = D_{NI} + G_{NI} \tag{20}$$

Where E_{NI} is the energy function and tests for existence of discontinuities in segmentation. D_{NI} is sum of distances between region center and surrounding pixels in this region. D_{NI} is the Euclidean distance obtained by Eq. (14). D_{NI} specifies spatial ambiguity in neutrosophic domain. To analyze D_{NI}, consider the fact that if there is small differences between neutrosophic sets which are within the segment, we will have small values for D_{NI}; consequently, the most homogeneous segment is introduced by the least value for D_{NI}.

G_{NI} specifies intensity ambiguity in gray scale domain and tests for belongingness of a pixel into a specified segment and is given by Eq. (21):

$$G_{NI} = \sum_{p \in R_i} |p - c(R_i)| \tag{21}$$

Where p defines intensity in original image img and $c(R_i)$ defines intensity of the centroid of region R_i. We find absolute difference for the whole pixels placed in region *i*. We can determine difference between pixel intensities in a specified segment using sum of absolute differences. To analyze G_{NI}, consider the fact that if there is much homogeneity between pixel intensities which are within a specified segment, we will have small values for G_{NI}; consequently, the most homogeneous segment is introduced by the least value for G_{NI}.

According to Eq. (20) and as discussed earlier, less value for E_{NI} determines more proper answer. It repeats for each of $hist_{max}(g_k)$, descending. In the following, we detect minimum value for E_{NI}, so we introduce the threshold as the one corresponding to the detected minimum of E_{NI} and name it as the optimal threshold ($optThresh$); $optThresh$ is used for image segmentation. This process results in creating two segments and hence, first iteration is done.

Set $itter = itter + 1$. There are two distinct regions considering $optThresh$ which are determined by $R_1 = [$ $minIntensity \ldots optThresh - 1]$ and$]maxIntensity + 1 \ldots optThresh = [R_2$. It continues until termination condition satisfies; consider Eq. (22):

$$\frac{\sum_{i=1}^{s} E_{NI_{R_i}}}{\delta^2(c(R_1),\ldots c(R_s))} \tag{22}$$

Where s is the number of gained segments until now, δ^2 is variance; therefore, energy of the whole gained segments is shown in numerator and variance of all segment centroids is shown in denominator. As we previously mentioned, we are seeking for less energy and besides more variances for segment centroids. Consequently, we aim to find less value for Eq. (22) which introduces more appropriate case.

The former routine continues while Eq. (22) gives less value in iteration $itter + 1$ rather than the value achieved in iteration $itter$, in other case, it terminates.

Our proposed segmentation algorithm is stated in table 1.

Table 1: Our proposed segmentation algorithm

Algorithm 2

Input: *an image* $img = [minIntensity \;\; maxIntensity]$

Output: *multi-class segmented image*

START

1. *Set* $itter = 1$ *and* $optThreshArray = \phi$
2. *Map* $img = [minIntensity \;\; maxIntensity]$ *into neutrosophic domain to generate* img_{NS} *using Eq. (9) to (13) (intensity is bounded from* $minIntensity$ *into* $maxIntensity$*).*
3. *Use Eq. (14) to measure distance between center pixel of a* $\lambda \times \lambda$ square in img_{NS} and its surrounding pixels in the square.
4. *Measure Eq. (16)-(18) to sort points of* $\lambda \times \lambda$ square in img_{NS} and select the median as ε.
5. *Find measured distances of step 3 which are less than* ε *and mark them.*
6. *Find intersection of marked pixels using Eq. (15).*
7. *Repeat step 3 to step 6 to process the whole image by moving* $\lambda \times \lambda$ *square from upper left of the image into downer right of that to generate* img_{NI}*.*
8. *Find local maximum of histogram of* img *named as* $hist_{max}(g_1)$, $hist_{max}(g_2)$, … ,$hist_{max}(g_k)$,….,$hist_{max}(g_n)$ *and sort the values descending.*
9. *For i=1 to n (n is the number of local maximum of histogram in current bounded intensities) do*
    - 9.1. *Consider* i^{th} *gray level corresponded to local maximum of histogram as a* $thresh$ *for segmentation, so, now there are two regions* $R_1 = [minIntensity \ldots thresh]$ and$]maxIntensity + 1 \ldots thresh = [R_2$.
    - 9.2. *Find center of two regions* R_1 *and* R_2 *by Eq. (19).*
    - 9.3. *Use Eq. (20) to find energy functions of regions* R_1 *and* R_2*.*
10. *Find the smallest value between energy functions measured at step 9, name it as* $optThresh$ *which is the best threshold for segmentation and add it to* $optThreshArray$ *which yields to* $hreshArray = optThreshArray \cup \{optThresh\}$ *, as a result, now there are two segments based on intensity value* $optThresh$*.*
11. *New sub images which need segmentation are* $R_1 = [minIntensity \ldots optThresh - 1]$ and $+1 \ldots optThresh = [R_2$

$maxIntensity$].

12. *Set* $itter = itter + 1$.

13. *Apply Eq. (22) to see whether to continue or not; if the obtained value is bigger than or equal to that of the last iteration, jump to step 15.*

14. *For each sub image repeat step 9 to 13.*

15. *Optimal thresholds are found in* $optThreshArray$*; apply this to segment the image.*

END

Dhar and Kundu (2021) mentioned to time consuming as one of the challenges in image segmentation; as a result, we propose a comparison between our approach's operation time and the one introduced by Dhar and Kundu (2021). We considered some images from various datasets. Fig. 10 illustrates the proposed comparison. As it is shown in Fig. 10, there is a remarkable difference between our proposed method's time consuming rather than the time needed for the method proposed by Dhar and Kundu (2021).

We have illustrated our results and presented a qualitative comparison between our approach and other segmentation methods in Fig. (10). Here, we are going to introduce some quantitative measures. RI (rand index) is obtained by Eq. (23) (Al-Dulaimi et al., 2016):

$$RI = 1 - \frac{a+b}{n(n-1)/2} \tag{23}$$

Where a shows the number of common pixels in segmented and ground truth images (note that these pixels belong to the same segments). b shows the number of pixels on segmented and ground truth images which are placed in various segments. n defines the number of pixels, totally.

RI tends to 1 for similar segmented image and ground truth image, whereas it tends to zero when there is no similarity between segmented image and ground truth image; consequently, RI close to 1 defines more accurate segmentation and RI close to zero defines less accurate segmentation.

SA (segmentation accuracy) is obtained by Eq. (24) (Li et al., 2011):

$$SA = \sum_i^c \frac{A_i \cup C_i}{\sum_{j=1}^{c} C_i} \tag{24}$$



518.835 27.213



548.777 12.809



440.182 16.909



592.592 20.814

(a) (b) (c)

Fig 10 Image segmentation considering their operation time; time is presented in seconds and is written on below of images. The four initial rows are from kaggle dataset and the rest are from Dhar and Kundu (2021) (column wise). (a) Original image. (b) Segmentation by Dhar and Kundu (2021). (c) segmentation by our proposed method

Where c determines the number of segments, A_i is the ith segment given by our proposed method and C_i is the i^{th} segment in ground truth image. SA determines the number of correctly segmented pixels with respect to the number of pixels, totally. As a result, bigger values for SA means more accurate segmentation and fewer values for SA means less accurate segmentation.

$F-Score$ which is obtained by Eq. (25) checks segmentation results' performance, quantitatively (Ziółko et al., 2018):

$$F-Score=\frac{2\times Pr\times Re}{Pr+Re} \tag{25}$$

$$Pr=\frac{TP}{TP+FP} \tag{26}$$

$$Re=\frac{TP}{TP+FN} \tag{27}$$

Where Pr and Re determine precision and recall for a segmented image related to ground truth, respectively and are obtained by Eq. (26) and (27). TP, FP and FN are true positive, false positive and false negative, respectively. More accurate segmentation is given by bigger values for $F-Score$ and less accurate segmentation is given by less values for $F-Score$.

Table 2 presents a comparison between our segmentation results and the results obtained from Dhar and Kundu (2021) for synthesized images. Table 3 presents a comparison between our segmentation results and the results obtained from Dhar and Kundu (2021) for nature images.

Table 2 quantitative comparison between segmentation by Dhar and Kundu (2021) and the proposed method for

synthesized images

Measure	Segmentation by Dhar and Kundu (2021)	Proposed method
RI	0.9502	0.9613
SA	0.9476	0.9601
F-Score	0.9528	0.9636

Table 3 quantitative comparison between segmentation by Dhar and Kundu (2021) and the proposed method for nature images

Measure	Segmentation by Dhar and Kundu (2021)	Proposed method
RI	0.8605	0.8927
SA	0.8581	0.8873
F-Score	0.8710	0.9101

3.4. Proposed image completion method

In this paper, we utilize Criminisi's exemplar-based image completion approach and extend it using the results of the already mentioned neutrosophic-based image segmentation algorithm. At the beginning, we segment the images using the predefined neutrosophic-based image segmentation algorithm, so that we have a segmented image. Two cases may appear for holes included in images:

(1) Hole is placed inside a distinct segment; it occurs when the all neighbourhood pixels belong to the same segment.
(2) Hole is not placed inside a distinct segment; it occurs when some neighbourhood pixels belong to different segments.

Case 1: As we explained in section 3.2, hole completion begins from outer pixels of target region. Therefore, we use Eq. (4) to determine these outer pixels' priority. Next, the pixel with the maximum priority is selected as $\boldsymbol{p}'$ used for $\boldsymbol{\Psi p}'$. In this approach, we set $\alpha = 9$ for patch size. We move from the centroid pixel into four-neighbourhood pixels and find whether there is a whole patch with the size α or not; if exists, the first patch founded $\boldsymbol{\Psi q}'$, is used to complete the hole. If it does not exists, we move across the current pixel's four

neighbourhood; it continues until we find a patch $\boldsymbol{\Psi q}'$ which is placed totally in similar segment as $\boldsymbol{\Psi p}'$. In some cases that moving across four neighbourhood of current pixel does not introduce a reasonable patch in the similar segment and at the same time, the patch is placed in more than one segment, go to case (2). It should be mentioned that $\boldsymbol{\Psi p}'$ has some known pixels and some unknown pixels which are named hole. As a result, only unknown pixels from $\boldsymbol{\Psi p}'$ are replaced with the corresponding pixels from $\boldsymbol{\Psi q}'$. In the following, confidence value is updated for all unknown pixels of $\boldsymbol{\Psi p}'$ using Eq. (8). It iterates until there is no pixel in target region. Note that this case appears when the whole hole is inside a singular segment.

Case 2: We again start hole completion from outer pixels of target region. We develop Eq. (4) to define these outer pixels' priority considering the number of adjacent segments for $\boldsymbol{\Psi p}$. We prioritize patch surrounded by less various segments, so, Eq. (4) is updated to Eq. (28).

$$P_{New}(p) = \frac{P(p)}{n} \tag{28}$$

Where $P(p)$ is the priority from Eq. (4) and n is the number of segments surrounded $\boldsymbol{\Psi p}$. whatever there are more various segments around the patch, n grows, which makes P_{New} falls down and contrariwise, whatever there are less various segments around the patch, n falls down, which makes P_{New} grows up. Consequently, the patch with more priority and at the same time, with less various segments around of it, is selected as $\boldsymbol{\Psi p}'$.

Since $\boldsymbol{\Psi p}'$ may be placed besides of some different segments, Eq. (29) is used to find $\boldsymbol{\Psi q}'$.

$$\boldsymbol{\Psi}_{q_T} = \arg\min_{\boldsymbol{\Psi}_q \in \Phi} a(\boldsymbol{\Psi}_p, \boldsymbol{\Psi}_q) \tag{29}$$

Where $a(\Psi_p, \Psi_q)$ is the sum of absolute differences of labeled segments of two patches Ψ_p and Ψ_q. Each segment has a distinct label so that if corresponding pixels are placed in similar segments, value 1 is set and if corresponding pixels are placed in different segments, value -1 is set. Sum of these values of an individual patch, defines this patch's score. The patch with minimum score is selected as $\boldsymbol{\Psi q}'$ which is used for completion.

We move from the centroid pixel $\boldsymbol{p}'$ into four-neighbourhood pixels and find the best match. Every seen pixel is marked in order to prevent re-checking. Each $\boldsymbol{\Psi q}$ is checked not to include hole. Consider $\boldsymbol{\Psi p}'$ has β known pixels. We set $\varepsilon = [0.95 * \beta]$ for acceptance rate; it means that after $\boldsymbol{\Psi q}_T$ is found, $a(\Psi_p, \Psi_{q_T})$ is compared to ε; for those values bigger than or equal to ε, the patch $\boldsymbol{\Psi q}_T$ is finally selected as $\boldsymbol{\Psi q}'$ to complete the hole. Yet, if the acceptance ratio is not satisfied, we keep the best patch ever found ($\boldsymbol{\Psi q}''$) and move forward in four-pixel neighbourhood of already seen pixels. If there are more than one patch which satisfy the acceptance rate, pixel intensity will be used to measure the sum of squared differences (SSD) of each of these patches and $\boldsymbol{\Psi p}'$. The patch with the minimum value for SSD is finally selected as $\boldsymbol{\Psi q}'$. If the acceptance rate is not satisfied, the best ever found patch $\boldsymbol{\Psi q}''$ will be considered as the best match $\boldsymbol{\Psi q}'$ and will be used to complete the hole. Then, only unknown pixels from $\boldsymbol{\Psi p}'$ are replaced with the corresponding pixels from $\boldsymbol{\Psi q}'$. In the following, confidence value is updated for all unknown pixels of $\boldsymbol{\Psi p}'$ using Eq. (8). It iterates until there is no pixel in target region. Here, we consider both neighbourhood information and similarity in this approach.

Here, our proposed image completion algorithm is stated in table 4. Fig. 11 (in Appendix) Depicts flowchart of the proposed method.

Table 4: Our proposed image completion algorithm

Algorithm 2

Part I) Segmentation:

Input: *an image* $img = [minIntensity \;\; maxIntensity]$

Output: *multi-class segmented image*

Use algorithm 1 to generate a segmented image which is used in part II.

Part II) Hole Completion:

Input: *an image containing a hole in it*

Output: *an image with the hole completed*

START

1. *Find priority of outer pixels of hole using Eq. (4)*
2. *Find the number of distinct adjacent segments (n) for each outer pixel of step 1*
3. *Find new priority value for outer pixels of hole using Eq. (28)*
4. *Select the pixel with maximum priority as* $\boldsymbol{p}'$ *and define the* 9×9 *patch* $\boldsymbol{\Psi p}'$ *as the selected patch for completion*
5. *If there is only one segment adjacent to* $\boldsymbol{p}'$*, then consider* $\boldsymbol{p}'$ *as the current pixel*

   Begin

   5.1. Movement Step: Move from the current pixel to its four neighbourhood

   5.2. If there is a 9×9 *patch completely placed in a similar segment to adjacent segment of* $\boldsymbol{\Psi p}'$*, and there is no unknown pixel in this patch, then*

   5.2.1. introduce it as $\boldsymbol{\Psi q}'$ *and go to step 7*

   Else if the above 9×9 *patch is placed in a similar segment to adjacent segment of* $\boldsymbol{\Psi p}'$*, but it contains some unknown pixels, then*

   5.2.2. Go to step 5.1 (Movement Step)

   Else (the above 9×9 *patch contains some various segments)*

   5.2.3. Go to step 6

   End

6. *If there are more than one distinct segment adjacent to* $\boldsymbol{p}'$*, then consider* $\boldsymbol{p}'$ *as the current pixel*

Begin

6.1. Movement Step: Move from the current pixel to its four neighbourhood

6.2. Use Eq. (29) to find the best patch between these four neighbourhood pixels

6.3. If $a(\Psi_p, \Psi_q)$ for the above best patch is bigger than or equal to $\varepsilon = [0.95 * \beta]$ and there is only one patch which satisfy the acceptance rate ε, then

6.3.1. Select the patch as Ψ_q'.

Else if $a(\Psi_p, \Psi_q)$ for the above best patch is bigger than or equal to $\varepsilon = [0.95 * \beta]$ and there are more than one patch which satisfy the acceptance rate ε, then

6.3.2. Use SSD to find the best match between these accepted patches and select the patch related to the smallest value for SSD as Ψ_q'.

Else If $a(\Psi_p, \Psi_q)$ for the above best patch is smaller than $\varepsilon = [0.95 * \beta]$ and there are also some neighbourhood pixels which are not met yet, then

6.3.3. keep the best ever found patch with minimum value for $a(\Psi_p, \Psi_q)$ named Ψ_q'' and go to step 6.1 (Movement Step)

Else ($a(\Psi_p, \Psi_q)$ for the above best patch is smaller than $\varepsilon = [0.95 * \beta]$ and there are not any neighbourhood pixels which are not met yet)

6.3.4. select Ψ_q'' as Ψ_q'

End

7. *complete the missing pixels of Ψ_p' using corresponding pixels in Ψ_q'*
8. *Update confidence value using Eq. (8)*
9. *If the hole is not totally completed, go to step 1*

END

4. Results and discussion

In this section, we illustrate our results and discuss the performance of proposed method. We also compare our results to some earlier ones. Results are compared both qualitatively and quantitatively. We initially show our results along with their saliency map to investigate whether our results get attention from viewers for completed hole or not. Next, we depict a qualitatively comparison of our results to formerly researches. In the following, we introduce some performance measures which help us to compare results quantitatively and then, we apply these measures to compare our results quantitatively to some earlier approaches.

Fig. 12 (which is continued in Appendix) shows results of image completion for some images. As you can see in Fig. 12, hole is depicted in green which is completed on third column. We showed saliency map of the completed image on the last column which emphasizes the completed hole makes no attention to the viewer. Saliency map is a quantitative model which gains the amount of viewers' attention to the image as a value and finds unexpected regions. Saliency map is obtained by filter-based models and the value of each pixel in saliency map is related to the amount of direct attention to that pixel's neighbourhood in a bounded time. We initially

gain feature maps using various filters, next, we set the contrast of these feature maps and sum them together using some weights for determination of the amount of viewer's attention. Finally, the acquired map is normalized between 0 and 1. The maximum and minimum values of saliency map is between 0 and 1; yet, we showed saliency map using different colours in which greater values that are illustrated in bold colours (red) are related to regions giving more attention to the viewer. As it is obvious in Fig. 12, there is no bold colours in saliency map in region corresponding to hole in the masked image; which means our completion result does not produce extra attention for the viewer.

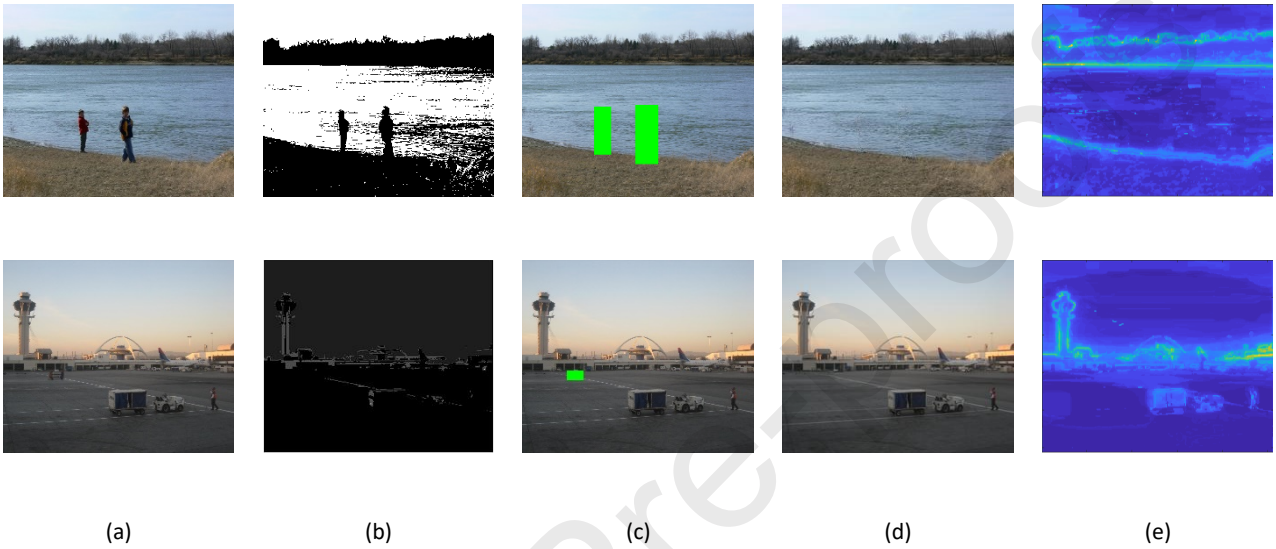

Fig. 12: saliency map for completed images. Images are taken from Li et al. (2022), Criminisi et al. (2004), Ghanbari, Talouki & Majdi (2019) and Giorgio (2018). (a) Original image (b) Segmented Image (c) Hole in green (d) Completed image (e) Saliency map for completed image

Fig. 13 (which is continued in Appendix) compares our completion results to results of Li et al. (2022). As you can see, our results are qualitatively more pleasant than results of Li et al. (2022). Yet, we introduce three quantitative measures in section 4.1 to 4.3 which are later used to compare our results to some earlier approaches.

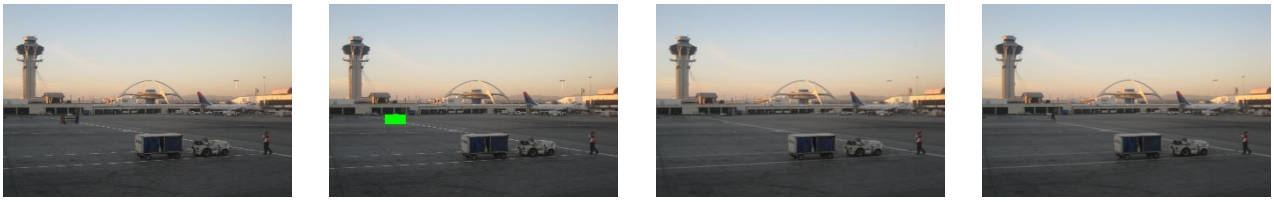

(a) (b) (c) (d)

Fig. 13: Comparision of our image completion results to results of Li et al. (2022). (a) Original images (b) Hole in green (c) Our completed image (d) image completion by Li et al. (2022)

4.1. ASVS (Average Squared Visual Salience)

$ASVS$ is about amount of error within the hole and is proposed as a value; this value is obtained from in-region distortions which appears when the completed target region gets direct attention from viewers. Therefore, less value for $in-region$ means better performance for the algorithm. In-region distortions is acquired from Eq. 30.

$$in-region(I) = \frac{1}{|\Omega|}\sum_{p \in \Omega}[S(p)]^2 \quad (30)$$

Where Ω is target region, I is the original image and $S(p)$ is saliency map for the completed image. Eq. 31 gives ASVS for image I.

$$ASVS(I) = in-region(I) \quad (31)$$

As it is clear, less value for $ASVS$ corresponds to less value for $in-region$ which means better completion for the target region (Ardis et al., 2009; Ardis et al., 2010). Fig. 14 (which is continued in Appendix) shows $ASVS$ for our results and method of Li et al. (2022). As it is obvious in Fig. 14, using neutrosophic-based image segmentation and performing image completion by considering neutrosophic sets brings us more pleasant result along with better qualitative and quantitative measures.

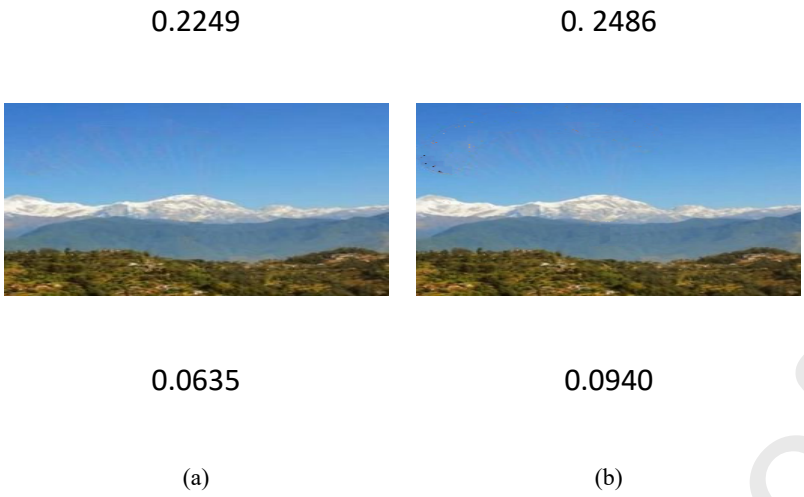

Fig. 14: Quantitative comparison of our results to Li et al. (2022) using ASVS. (a) Our results (b) Results of Li et al. (2022). ASVS are written in bottom of each completed image

4.2. SSIM (Structure Similarity)

This measure was proposed by Wang et al., (2004) to bring out a quantitative measure to compare image completion results while original image exists. Eq. (32) introduces $SSIM$ index.

$$SSIM(x,y) = [l(x,y)]^{\alpha}.[c(x,y)]^{\beta}.[s(x,y)]^{\lambda} \tag{32}$$

Where $l(x,y)$, $c(x,y)$ and $s(x,y)$ are luminance, contrast and structure of two images, respectively and are obtained from Eq. (33) to Eq. (35).

$$l(x,y) = \frac{2\mu_x\mu_y + C_1}{\mu_x^2 + \mu_y^2 + C_1} \tag{33}$$

$$c(x,y) = \frac{2\sigma_x\sigma_y + C_2}{\sigma_x^2 + \sigma_y^2 + C_2} \tag{34}$$

$$s(x,y) = \frac{\sigma_{xy} + C_3}{\sigma_x.\sigma_y + C_3} \tag{35}$$

If we set $\alpha = \beta = \lambda = 1$ and $C_3 = C_2/2$ in Eq. (32), then we have Eq. (36) for $SSIM$:

$$SSIM(x,y) = \frac{(2\mu_x\mu_y + C_1)(2\sigma_x\sigma_y + C_2)}{(\mu_x^2 + \mu_y^2 + C_1)(\sigma_x^2 + \sigma_y^2 + C_2)} \quad (36)$$

C_1 and C_2 are constants for sustainability. As it is obvious in Eq. (33) to (35), luminance and contrast are given by mean and variance of pixels; yet, covariance is used for structure. It should be mentioned that these values are obtained for different corresponding windows for two images: original image and destroyed image. Since there are too many values according to number of windows, mean of $SSIM$ for windows is used as a comparing measure for an image which is given by Eq. (37):

$$MSSIM(X,Y) = \frac{1}{M}\sum_{j=1}^{M} SSIM(x_j,y_j) \quad (37)$$

Where X is the original image, Y is the destroyed image, M is the number of windows and x_j and y_j are pixels of j^{th} window in image. $MSSIM$ is one for two similar images, therefore, whatever the acquired $MSSIM$ is closer to one, it means there is more similarity between two images.

Table 5 compares $MSSIM$ for our results compared to some earlier researches for images in Fig. 12. As you can see, the proposed method introduces the greatest value between all values in table 5 which means the completed image is the most similar one into the original image considering all other researches' results; because neutrosophic sets consider indeterminacy exists in images and brings forward a more satisfactory segmented image which leads to a more satisfactory completed image.

Table 5: Comparison of our result to earlier researches based on $MSSIM$ index

Criminisi et al. (2004)	Yao (2019)	Zhang et al. (2014)	Darabi et al. (2012)	Zhang et al. (2019)	Li et al. (2022)	Our
0.9856	0.9848	0.9750	0.9707	0.9886	0.8929	0.9919

Fig. 15 illustrates an original image along with inpainted results using different algorithms proposed by researches which are mentioned in table 5.

(a) (b) (c) (d) (e) (f) (g) (h)

Fig. 15: Comparision of our image completion results to some earlier researches. (a) Original images (b) image completion by Criminisi et al., (2004) (c) image completion by Yao, (2019) (d) image completion by Zhang et al., (2014) (e) image completion by Darabi et al., (2012) (f) image completion by Zhang et al., (2019) (g) image completion by Li et al., (2022) (h) Our completed image.

4.3. PSNR (Peak Signal to Noise Ratio)

One of the most important measures for image quality evaluation is $PSNR$ which is given by Eq. (38) and (39):

$$MSE = \frac{1}{M.N}\sum_{i=1}^{m}\sum_{j=1}^{n}\|I(i,j) - M(i,j)\|^2 \quad (38)$$

$$PSNR = 10.\log\left(\frac{255^2}{\sqrt{MSE}}\right) \quad (39)$$

Where MSE is mean square error, m and n are image dimensions and $I(i,j)$ and $M(i,j)$ are pixels of original image and completed image, respectively (Wang et al., 2002).

Table 6 compares $PSNR$ for our results compared to some earlier researches. As it is clear in Eq. (38) and Eq. (39), whatever two images (original image and the completed one) are similar to each other, there is less difference between them; therefore the less MSE will be obtained. Since MSE is the denominator in $PSNR$ formula, whatever we have less value for MSE, we will have more value for $PSNR$. Values in table 6 emphasises the proposed neutrosophic-based image completion method which applies neutrosophic-based image segmentation introduces greater value for $PSNR$ which inherently means better completion result and it is owed to neutrosophic sets's property to decreases spatial and intensity ambiguities of images and bringing forward segmented images with more boundary and homogeneity preserving in addition to less discontinuity.

Table 6: Comparison of our result to earlier researches based on $PSNR$ index

Criminisi et al. (2004)	Yao (2019)	Zhang et al. (2014)	Darabi et al. (2012)	Zhang et al. (2019)	Li et al. (2022)	Our
28.16	36.75	24.98	21.37	29.60	33.98	38.96

Fig. 16 compares $ASVS$ for our results to two other researches; Shajahan et al., (2019). Table 7 shows a comparison for $MSSIM$ and $PSNR$ between our results and Shajahan et al., (2019).

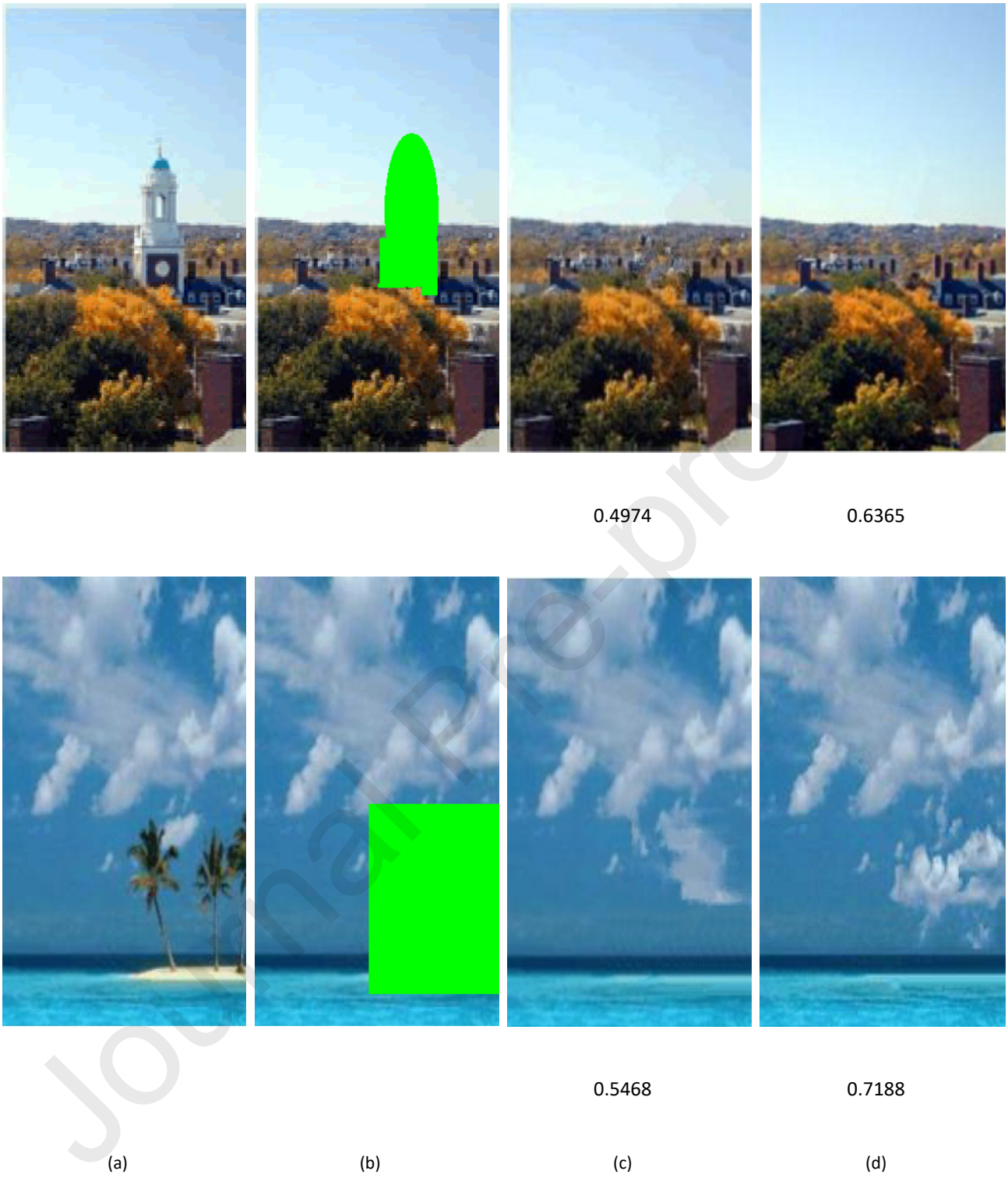

Fig. 16: Quantitative comparison of our results to Shajahan et al., (2019) using $ASVS$. (a) Original image (b) Hole in green (c) Our completed image (d) Image completion by Shajahan et al., (2019) $ASVS$ are written in bottom of each completed image

Table 7: Comparison of our result to Shajahan et al., (2019) based on $MSSIM$ and $PSNR$ index

	$MSSIM$	$PSNR$
Shajahan et al., (2019)	0.8249	30.6257
Our method	0.9359	33.4901

Fig. 17 compares $ASVS$ for our results to two other researches; Zhao et al., (2022). Table 8 shows a comparison for $MSSIM$ and $PSNR$ between our results and Zhao et al., (2022).

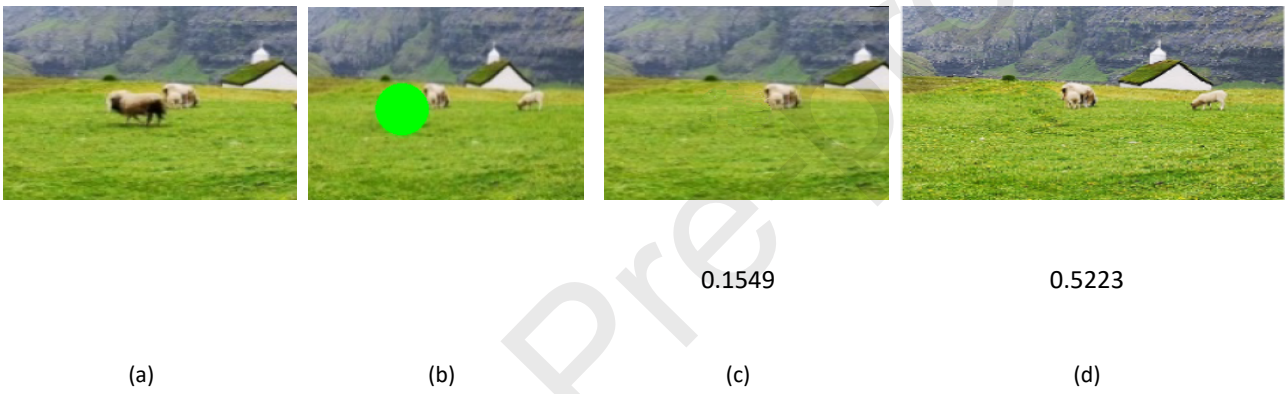

Fig. 17: Quantitative comparison of our results to Zhao et al., (2022) using $ASVS$. (a) Original image (b) Hole in green (c) Our completed image (d) Image completion by Zhao et al., (2022) $ASVS$ are written in bottom of each completed image

Table 8: Comparison of our result to Zhao et al., (2022) based on $MSSIM$ and $PSNR$ index

	$MSSIM$	$PSNR$
Zhao et al., (2022)	0.5878	32.1277
Our method	0.9210	35.2472

5. Conclusion

Image completion follows the aim of retrieving old damaged images and nowadays is a copacetic subject in image processing and computer vision. Holes in destroyed images are completed using a similarity measure which aims to find the most appropriate data for hole completion; finding this most suitable data is an important

challenge which affects completion results because it is very important to maintain the visual consistency in completion process and in this case, using wrong information for hole completion makes the results unpleasant. In this paper, we proposed a novel exemplar-based image completion method which uses neutrosophic sets to segment an image and applies segmentation information along with similarity measures which consider both neighbourhood and similarity information to find the most appropriate match to complete the hole.

The novelty of our algorithm compared to earlier researches is that we completed damaged images using patches which were the best available in images according to our extended similarity measure which consider both neighbourhood and similarity based on results of our innovative image segmentation approach. Our neutrosophic-based image segmentation algorithm decreases spatial and intensity ambiguities of images and guides us to have segmented images with more boundary and homogeneity preserving in addition to less discontinuity which introduces an improvement in RI, SA and $F\text{-}Score$ compared to earlier researches. The proposed image completion method benefits of more satisfactory results according to qualitative and quantitative measures. Our approach introduces an improvement of 18% for $ASVS$ compared to earlier methods. We also gained 0.9919 and 38.96 for $MSSIM$ and $PSNR$, respectively while the best values for earlier methods were 0.9868 and 36.75 for $MSSIM$ and $PSNR$, respectively which is the effect of using neutrosophic segmentation.

The proposed method presents well performance for corrupted images qualitatively and quantitatively compared to formerly introduced researches. We did not consider noise in the current research, nor camera jitter which they can be considered in future researches. Therefore, we compared our results to researches which they did not tackle with noise, too. We are also going to include corrupted video frames which are needed to be repaired either considering static scenes or dynamic ones to our future studies.

references

Ahmed, H. O., Alfaqheri, T., & Sadka, A. H. (2021). Digital Image Inpainting Techniques for Cultural Heritage Preservation and Restoration. *In Data Analytics for Cultural Heritage*. *Springer*, Cham, 91-122.

Al-Dulaimi, K., Tomeo-Reyes, I., Banks, J., & Chandran, V. (2016, November). White blood cell nuclei segmentation using level set methods and geometric active contours. In 2016 international conference on digital image computing: techniques and applications (DICTA), 1-7, IEEE. DOI: 10.1109/DICTA.2016.7797097

Ardis, P. A., Brown, C. M., & Singhal, A. (2010). Inpainting quality assessment. Journal of Electronic Imaging, 19(1), 011002.

Ardis, P. A., & Singhal, A. (2009, January). Visual salience metrics for image inpainting. In Visual Communications and Image Processing *2009*, 7257, 606-614). SPIE.

Bertalmio, M., Sapiro, G. & Ballester, C. (2002). Image Inpainting. *In Proceedings of the 27th annual conference on Computer graphics and interactive techniques (SIGGRAPH '00)*, 417–424. DOI:https://doi.org/10.1145/344779.344972.

Broumi S., Bakali A., Talea M., Smarandache F., Uluçay V., Sahin M., ... & Pramanik S. (2018). Neutrosophic Sets: An Overview. *New Trends in Neutrosophic Theory and Applications*. 2, 403.

Chen, Y., Wang, M., Heidari, A. A., Shi, B., Hu, Z., Zhang, Q., ... & Turabieh, H. (2022). Multi-threshold image segmentation using a multi-strategy shuffled frog leaping algorithm. *Expert Systems with Applications*, 194, 116511. https://doi.org/10.1016/j.eswa.2022.116511

Cherel, N., Almansa, A., Gousseau, Y., & Newson, A. (2022). Patch-Based Stochastic Attention for Image Editing. *arXiv preprint arXiv*:2202.03163.

Cho, J., Kang, M., Vineet, V., & Park, J. (2022). Context-Aware Image Completion. *arXiv preprint arXiv*:2210.12350.

Criminisi, A., Pérez, P., & Toyama, K. (2004). Region filling and object removal by exemplar-based image inpainting. *IEEE Transactions on image processing*, 13(9), 1200-1212.

Darabi, S., Shechtman, E., Barnes, C., Goldman, D. B., & Sen, P. (2012). Image melding: Combining inconsistent images using patch-based synthesis. *ACM Transactions on graphics (TOG)*, 31(4), 1-10.

Dhar, S., Kundu, M. K. (2021). Accurate multi-class image segmentation using weak continuity constraints and neutrosophic set. *Applied Soft Computing*, 112, 107759. https://doi.org/10.1016/j.asoc.2021.107759

Ding, T., Sznaier, M., & Camps, O. I. (2007). A rank minimization approach to video inpainting. *Proceedings of IEEE*

Conference on Computer Vision, 1–8, 10.1109/ICCV.2007.4408932.
Dou, L., Qian, Z., Qin, C., Feng, G., & Zhang, X. (2020). Anti-forensics of diffusion-based image inpainting. *Journal of Electronic Imaging*, 29(4), 043026.
Ghanbari, Talouki, A., Koochari, A., & Edalatpanah, S. A. (2021). Applications of neutrosophic logic in image processing: A survey. *Journal of Electrical and Computer Engineering Innovations (JECEI)*, 10(1), 243-258.
Ghanbari, Talouki, A. & Majdi, M. (2019). Improvement in Video Inpainting in Presence of Moving Subject. *International Journal of Research in Industrial Engineering*, 8(4), 320-333.
Ghanbari, Talouki, A., Majdi, M. & Edalatpanah, S. A. (2017). An Introduction to Various Algorithms for Video Completion and Their Features: A Survey. *Journal of Computer Sciences and Applications*, 5(1), 1-10.
Ghanbari Talouki, A. & Soryani, M. (2011). Contour based video inpainting. *Presented at the IEEE conference on Machine Vision and Image Processing*, 10.1109/IranianMVIP.2011.6121586.
Guo, Y. & Cheng, H.D. (2009).A new neutrosophic approach to image denoising. *New Mathematics and Natural Computation (NMNC)*, 5(3), 653-662.
Giorgio C. (2018), https://drive.google.com/file/d/1HzDyyoMPvGw3fs-dP63o39v7-9LjKpaF/view?usp=share_link
Hu, K., & Fan, E. (2017). A New Algorithm for Improving Basic Model Based Foreground Detection Using Neutrosophic Similarity Score. *Infinite Study*.
Irvanizam, I., Syahrini, I., Zi, N. N., Azzahra, N., Iqbal, M., Marzuki, M., & Subianto, M. (2021). An improved EDAS method based on bipolar neutrosophic set and its application in group decision-making. *Applied Computational Intelligence and Soft Computing*, *2021*, 1-16.
Irvanizam, I., Zulfan, Z., Nasir, P. F., Marzuki, M., Rusdiana, S., & Salwa, N. (2022). An extended MULTIMOORA based on trapezoidal fuzzy neutrosophic sets and objective weighting method in group decision-making. *IEEE Access*, 10, 47476-47498.
Jayachandran, A., & Dhanasekaran, R. (2013). Automatic detection of brain tumor in magnetic resonance images using multi-texton histogram and support vector machine. *International Journal of Imaging Systems and Technology*, 23(2), 97-103.
Jia, J., Tai, Y., Wu, T., & Tang, C. (2006). Video repairing under variable illumination using cyclic motions. *IEEE Transactions on Pattern Analysis and Machine Intelligence*, 28(5), 832–883.
Jo, Y., & Park, J. (2019). Sc-fegan: Face editing generative adversarial network with user's sketch and color. *In Proceedings of the IEEE/CVF international conference on computer vision*, 1745-1753.
Kaggle dataset: https://www.kaggle.com/code/ahmadsayed/first-ss/notebook
Li, C., Chen, H., Han, X., Pan, X., & Niu, D. (2022, April). An improved Criminisi method for image inpainting. *In Journal of Physics: Conference Series*, *IOP Publishing*, 2253(1), 012023.
Li, P., & Chen, Y. (2022). Research into an image inpainting algorithm via multilevel attention progression mechanism. *Mathematical Problems in Engineering*, 2022, 1-12.
Li, C., Huang, R., Ding, Z., Gatenby, J. C., Metaxas, D. N., & Gore, J. C. (2011). A level set method for image segmentation in the presence of intensity inhomogeneities with application to MRI. *IEEE transactions on image processing*, 20(7), 2007-2016. DOI: 10.1109/TIP.2011.2146190
Li, H., Luo, W., & Huang, J. (2017). Localization of diffusion-based inpainting in digital images. *IEEE transactions on information forensics and security*, 12(12), 3050-3064.
Ling, C. H., Liang, Y. M., Lin, C. W., Chen, Y. S., & Liao, H. Y. M. (2011). Human object inpainting using manifold learning-based posture sequence estimation. *IEEE Transactions on Image Processing*, 20(11), 3124 – 3135.
Luo, X., Wang, G., Liao, W., Chen, J., Song, T., Chen, Y., Zhang, S., Metaxas, D. N., Zhang, S. (2022). Semi-supervised medical image segmentation via uncertainty rectified pyramid consistency. *Medical Image Analysis*, 80, 102517. https://doi.org/10.1016/j.media.2022.102517
Mousavi, S. M. H., & Mosavi, S. M. H. (2022, March). A New Edge and Pixel-Based Image Quality Assessment Metric for Colour and Depth Images. *In 2022 9th Iranian Joint Congress on Fuzzy and Intelligent Systems (CFIS)*, 1-11.
Newson, A., Almansa, A., Fradet, M., Gousseau, Y. & Pérez, P. (2014). Video Inpainting of Complex Scenes. *SIAM Journal on Imaging Sciences, Society for Industrial and Applied Mathematics*, 7(4), 1993-2019.
Prasath, V. B., & Delhibabu, R. (2014, December). Image Inpainting with Modified F-Transform. *In International Conference on Swarm, Evolutionary, and Memetic Computing, Springer*, Cham, 856-867.
Quan, W., Zhang, R., Zhang, Y., Li, Z., Wang, J., & Yan, D. M. (2022). Image inpainting with local and global refinement. *IEEE Transactions on Image Processing*, 31, 2405-2420.
Romero, A., Castillo, A., Abril-Nova, J., Timofte, R., Das, R., Hira, S., ... & Huang, H. (2022). NTIRE 2022 image inpainting challenge: Report. *In Proceedings of the IEEE/CVF Conference on Computer Vision and Pattern Recognition* , 1150-1182.
Salama, A., Smarandache, F., & Eisa, M. (2014). Introduction to Image Processing via Neutrosophic Techniques. *Neutrosophic Sets and Systems*. 5, 59-64. DOI:10.5281/zenodo.30198.
Shajahan, S., Kumar, R. M. S., & Raj, J. V. (2019). Direction Oriented Block based Inpainting using Morphological Operations, *International Journal of Innovative Technology and Exploring Engineering (IJITEE)*, 8(12), 2769-2774.
Shroff, M., Bombaywala, M., & Salman, R. (2019). A qualitative study of exemplar based image inpainting. *SN Applied*

Sciences, 1(12), 1-8.
Smarandache, F. (1998). Neutrosophy: neutrosophic probability, set, and logic: analytic synthesis & synthetic analysis. *American Research Pressl*. 105.
Smarandache, F., Quiroz-Martínez, M. A., Ricardo, J. E., Hernández, N. B., & Vázquez, M. Y. L. (2020). Application of neutrosophic offsets for digital image processing. *Infinite Study*.
Song, S., Jia, Z., Yang, J., & Kasabov, N. K. (2020). A fast image segmentation algorithm based on saliency map and neutrosophic set theory. *IEEE Photonics Journal*, 12(5), 1-16.
Sufyan, M. & Badnerkar, S. (2015). Unwanted Object Removal In A Video By Using Video Inpainting Technique. *International Journal of Advanced Research in Electronics and Communication Engineering (IJARECE)*, 4(2), 407-410.
Tran, M.-T.; Kim, S.-H.; Yang, H.-J.; Lee, G.-S. (2021). Multi-Task Learning for Medical Image Inpainting Based on Organ Boundary Awareness. *Appl. Sci.* 2021, *11*, 4247. https://doi.org/10.3390/app11094247
Wang, Z., Bovik, A. C., Sheikh, H. R., & Simoncelli, E. P. (2004). Image quality assessment: from error visibility to structural similarity. IEEE transactions on image processing, 13(4), 600-612.
Wang, Y., Ostermann, J., & Zhang, Y. Q. (2002). Video processing and communications. *Pearson* (1st ed.).
Xu, G., Wang, S., Yang, T.,,Jiang, W. (2018). A neutrosophic approach based on TOPSIS method to image segmentation. *International Journal of Computers Communications & Control*. 13(6), 1047-1061. http://orcid.org/0000-0001-5429-2748
Yan, Z., Li, X., Li, M., Zuo, W., & Shan, S. (2018). Shift-net: Image inpainting via deep feature rearrangement. *In Proceedings of the European conference on computer vision (ECCV)* (1-17).
Yao, F. (2019). Damaged region filling by improved criminisi image inpainting algorithm for thangka. *Cluster Computing*, 22(6), 13683-13691.
Ye, J. (2014). Similarity measures between interval neutrosophic sets and their applications in multicriteria decision-making. *J. Intell. Fuzzy Syst*. 26, 165–172. DOI: 10.3233/IFS-120724
Zhang, N., Ji, H., Liu, L., & Wang, G. (2019). Exemplar-based image inpainting using angle-aware patch matching. *EURASIP Journal on Image and Video Processing*, 2019(1), 1-13.
Zhang, J., Zhao, D., & Gao, W. (2014). Group-based sparse representation for image restoration. *IEEE transactions on image processing*, 23(8), 3336-3351.
Zhao, J., Tan, J., Huang, Y., & Lu, C. (2022). Improved image inpainting exemplar-based algorithms by boundary priori-knowledge. *In MATEC Web of Conferences, EDP Sciences*, 355.
Zhou, T., Johnson, B., & Li, R. (2016). Patch-based texture synthesis for image inpainting. *arXiv preprint arXiv*:1605.01576.
Ziółko, B., Emms, D., Ziółko, M. (2018). Fuzzy evaluations of image segmentations. *IEEE Transactions on Fuzzy Systems*, 26(4), 1789-1799. DOI: 10.1109/TFUZZ.2017.2752130

Appendix

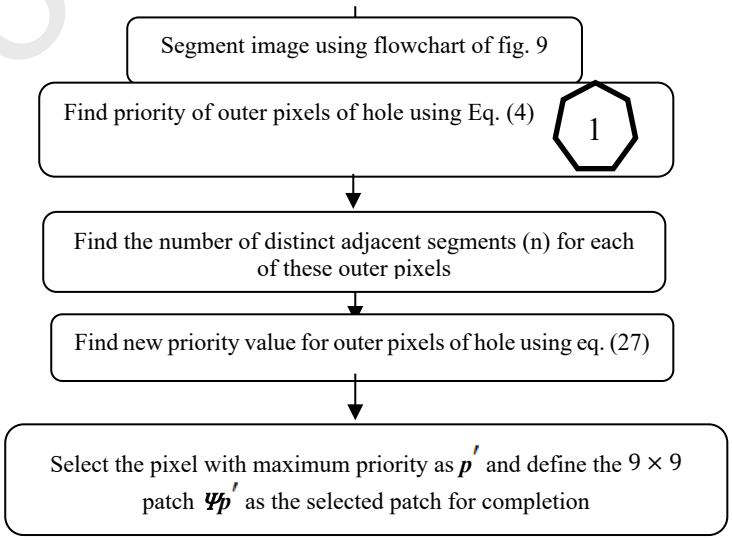

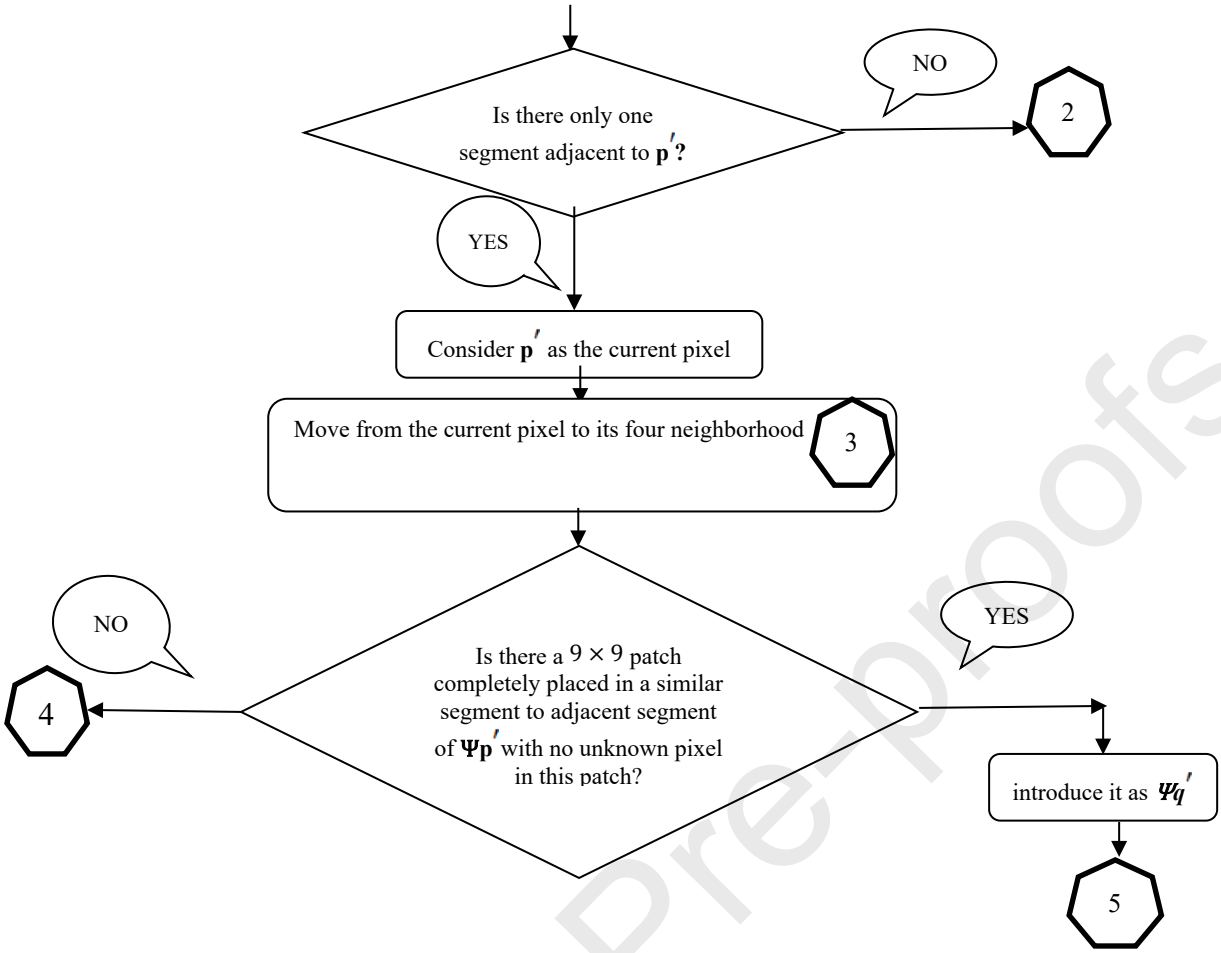

Fig. 11: flowchart of the proposed method (continued)

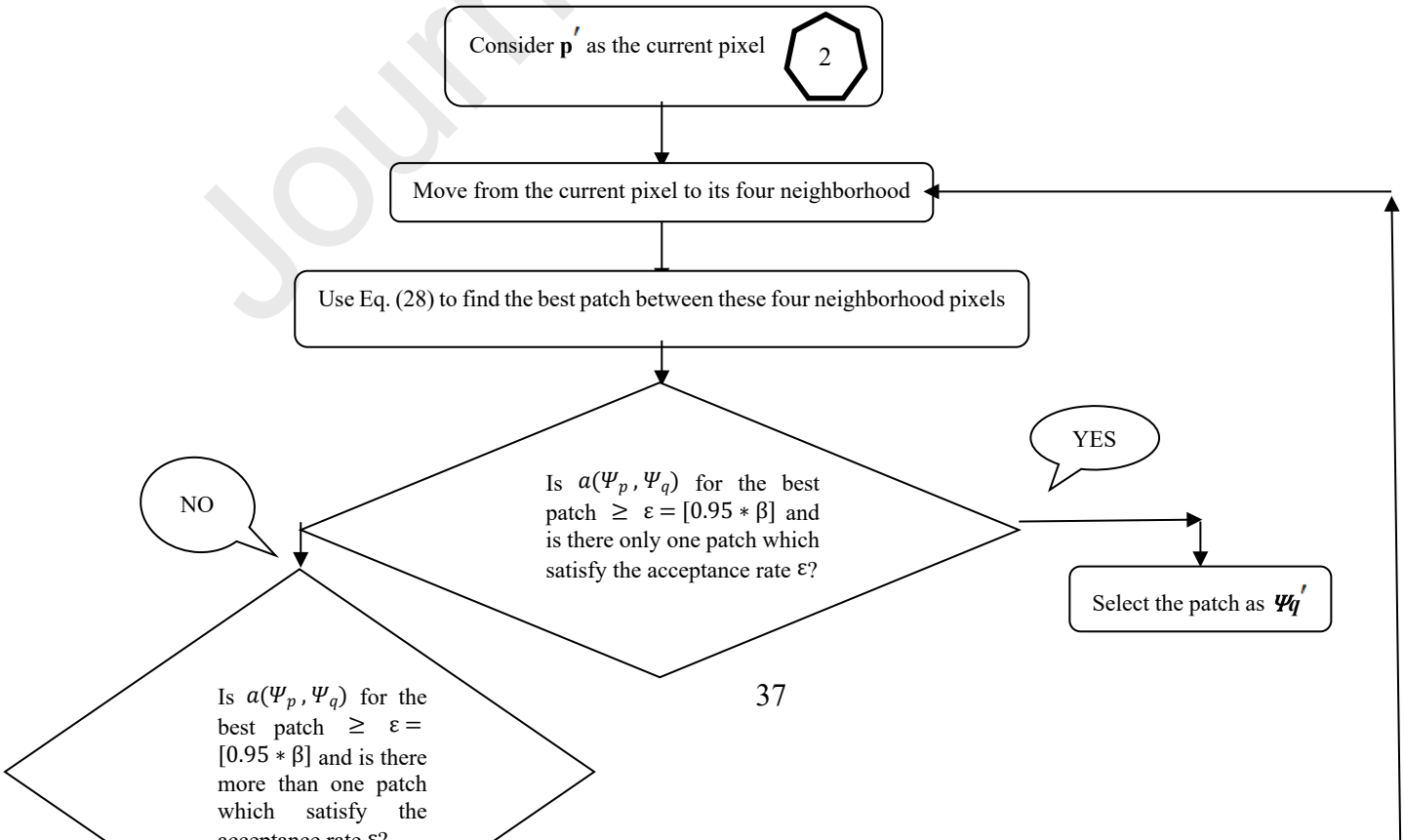

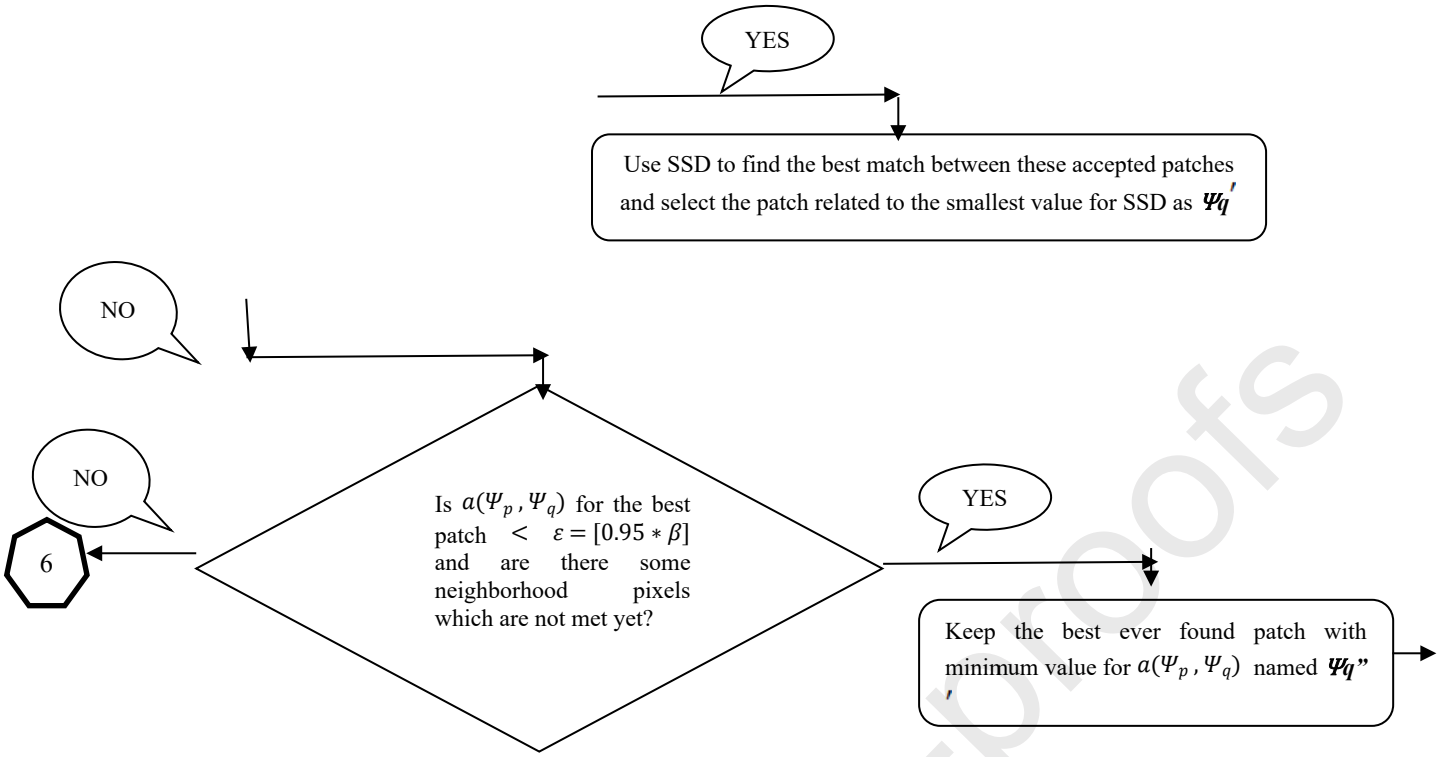

Fig. 11: flowchart of the proposed method (continued)

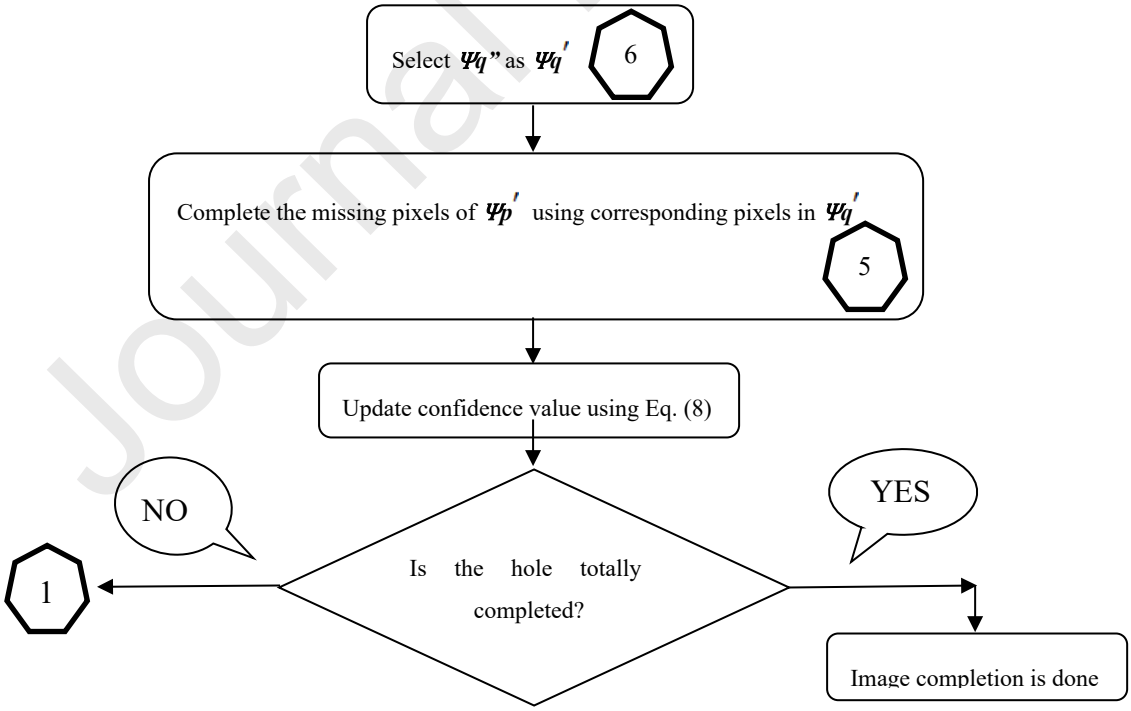

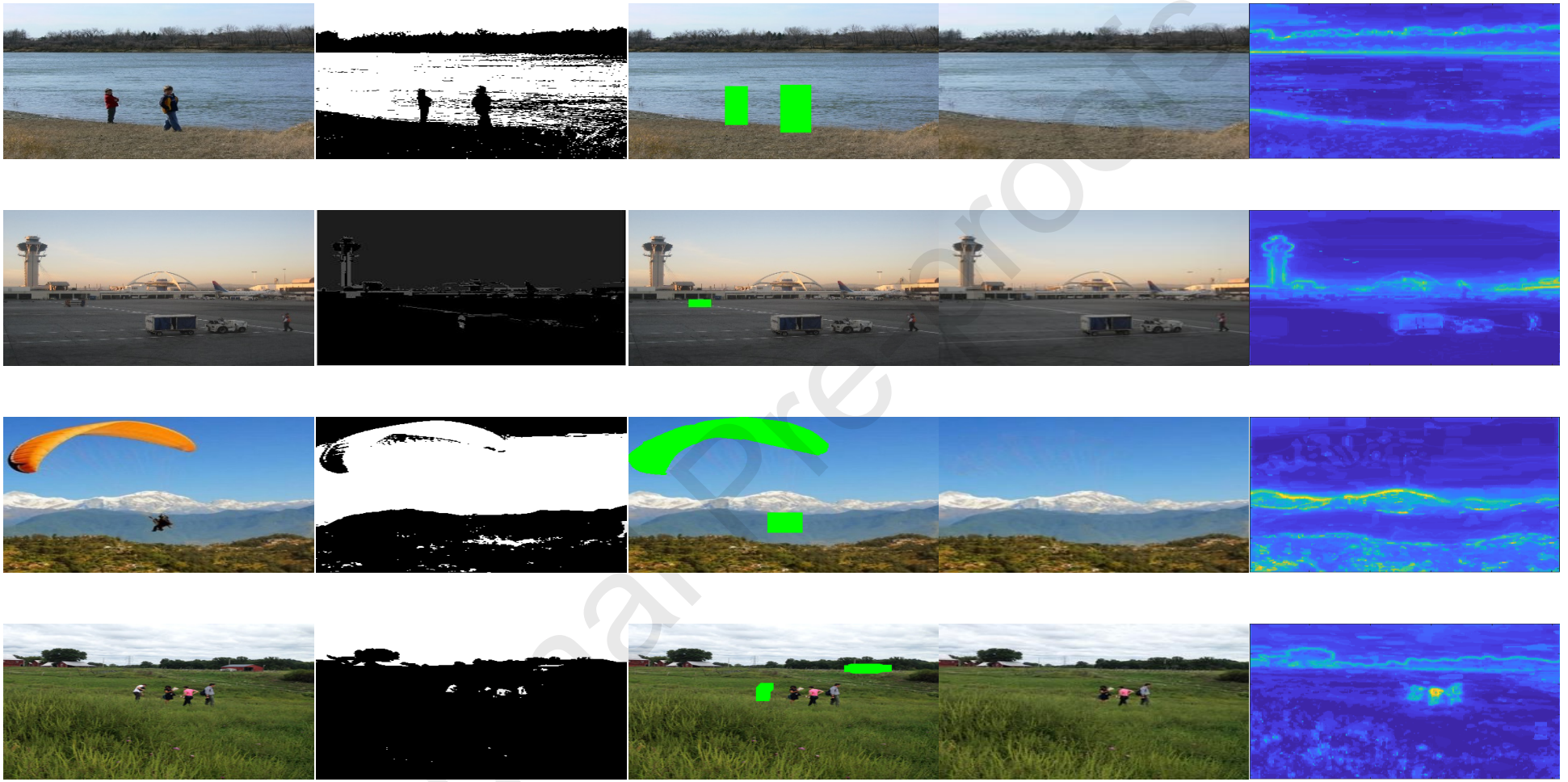

(a) (b) (c) (d) (e)

Fig. 12: saliency map for completed images. Images are taken from Li et al. (2022), Criminisi et al. (2004), Ghanbari, Talouki & Majdi (2019) and Giorgio (2018) (a) Original image (b) Segmented Image (c) Hole in green (d) Completed image (e) Saliency map for completed image (continued)

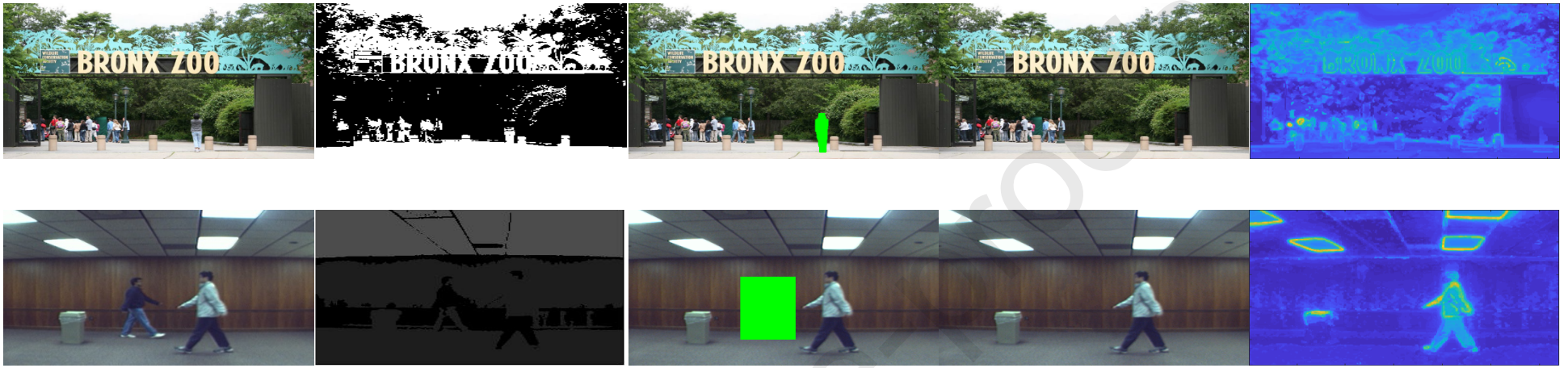

(a) (b) (c) (d) (e)

Fig. 12: saliency map for completed images. Images are taken from Li et al. (2022), Criminisi et al. (2004), Ghanbari, Talouki & Majdi (2019) and Giorgio (2018) (a) Original image (b) Segmented Image (c) Hole in green (d) Completed image (e) Saliency map for completed image (continued)

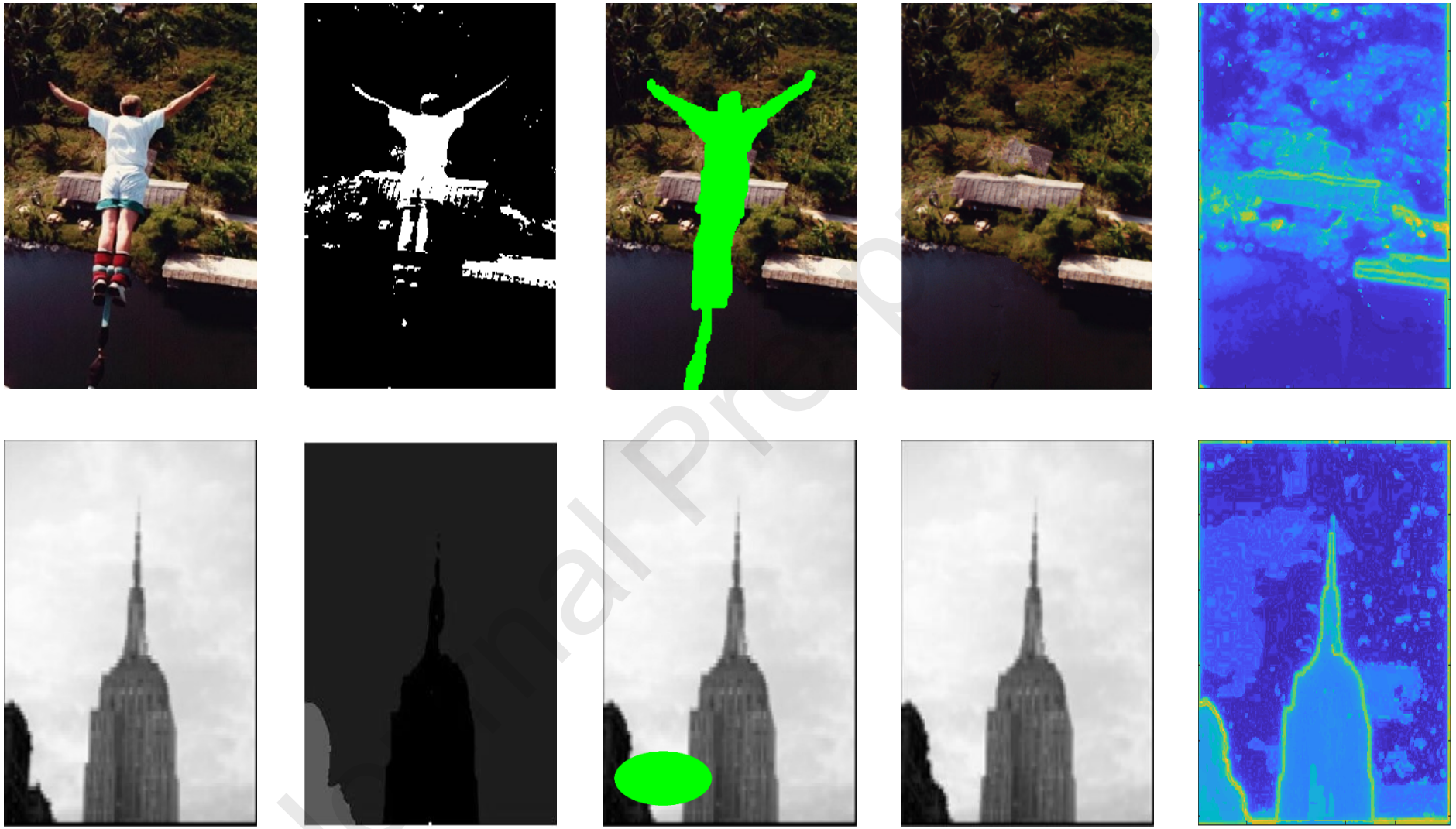

(a) (b) (c) (d) (e)

Fig. 12: saliency map for completed images. Images are taken from Li et al. (2022), Criminisi et al. (2004), Ghanbari, Talouki & Majdi (2019) and Giorgio (2018) (a) Original image (b) Segmented Image (c) Hole in green (d) Completed image (e) Saliency map for completed image

(a) (b) (c) (d)

Fig. 13: Comparision of our image completion results to results of [30]. (a) Original images (b) Hole in green (c) Our completed image (d) image completion by Li et al., (2022). (continued)

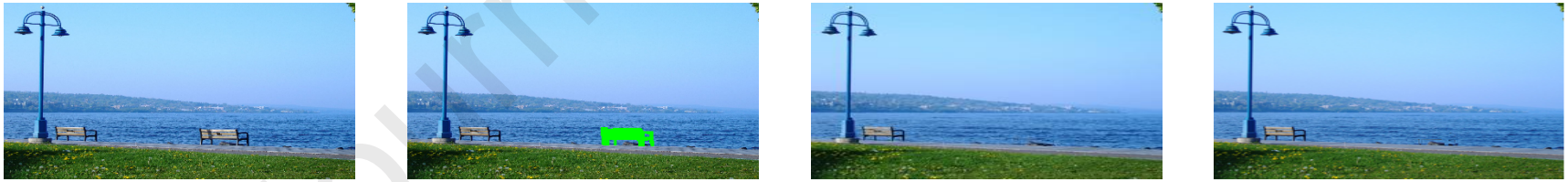

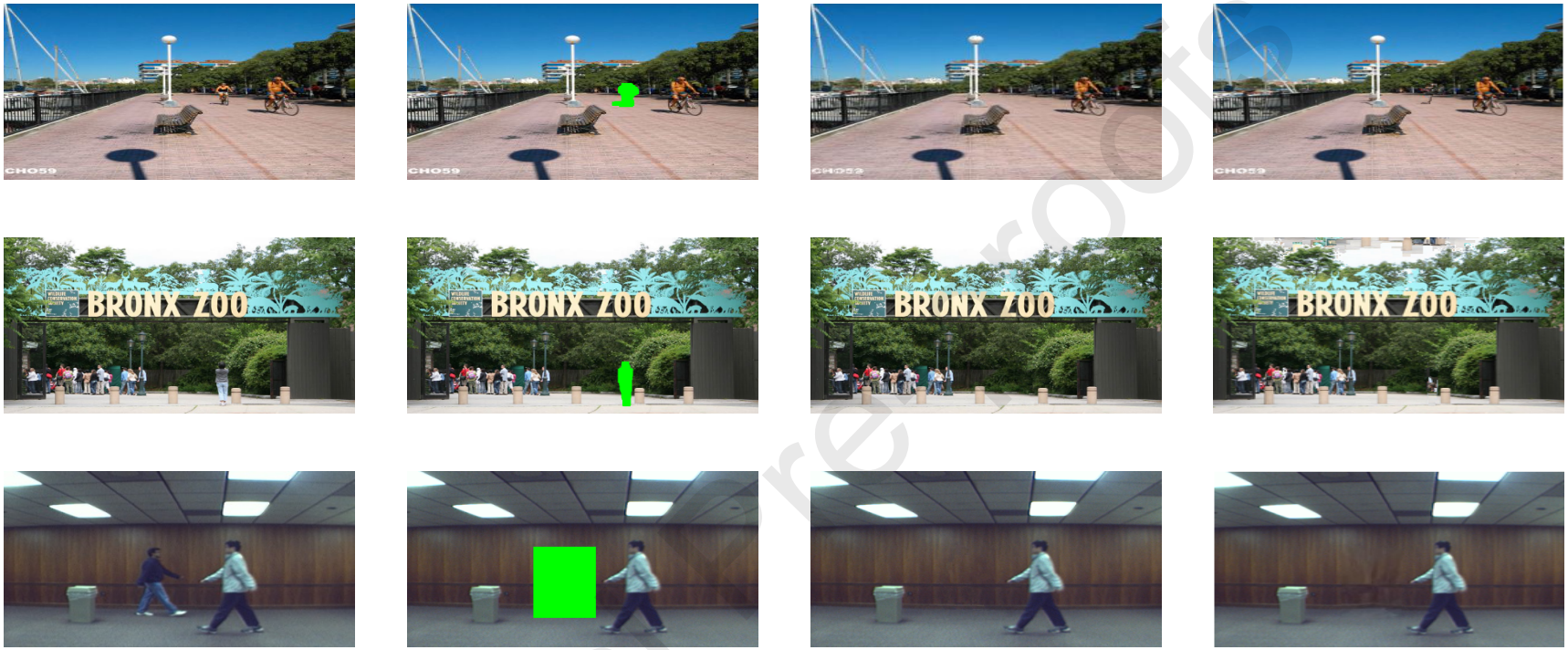

(a) (b) (c) (d)

Fig. 13: Comparision of our image completion results to results of [30]. (a) Original images (b) Hole in green (c) Our completed image (d) image completion by Li et al., (2022). (continued)

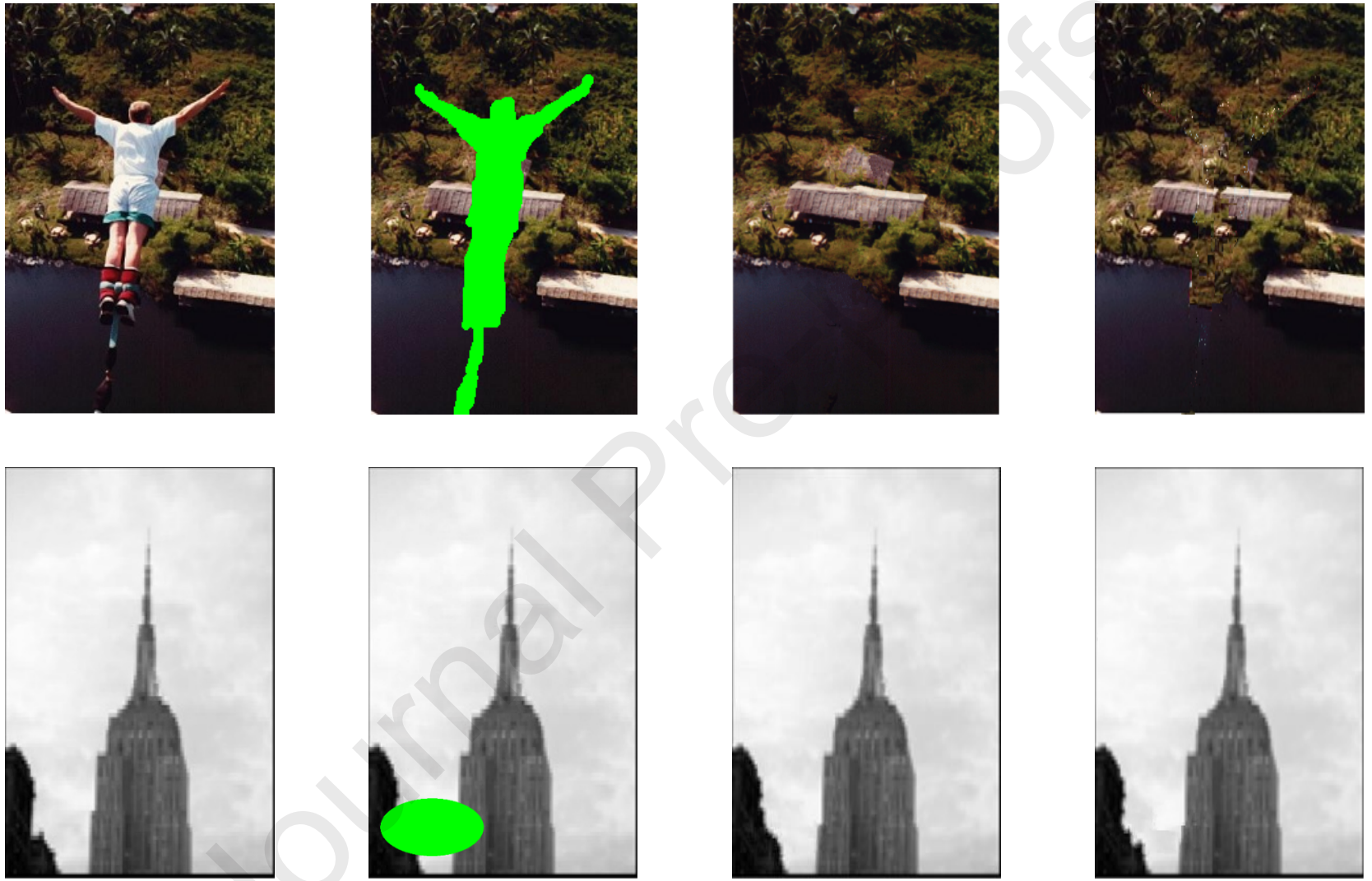

(a) (b) (c) (d)

Fig. 13: Comparision of our image completion results to results of [30]. (a) Original images (b) Hole in green (c) Our completed image (d) image completion by Li et al., (2022).




0.4614 0.3886 0. 2486 0.2249




1.1419 1.0520 0.0940 0.0635




Fig. 14: Quantitative comparison of our results to Li et al., (2022) using ASVS. (a) and (c) Results of Li et al., (2022). (b) and (d) Our results. ASVS are written in bottom of each completed image (continued)

1.0258 0.9607 1.3682 1.0843

(a) (b) (c) (d)

Fig. 14: Quantitative comparison of our results to Li et al., (2022) using ASVS. (a) and (c) Results of Li et al., (2022). (b) and (d) Our results. ASVS are written in bottom of each completed image

`

Authors' contributions are as follows.

Conceptualization: A. Ghanbari Talouki, A. Koochari, S. A. Edalatpanah; **Methodology**: A. Ghanbari Talouki, A. Koochari, S. A. Edalatpanah; **Software**: A. Ghanbari Talouki; **Validation**: A. Ghanbari Talouki, A. Koochari; **Formal analysis**: A. Ghanbari Talouki, A. Koochari; **Investigation**: A. Ghanbari Talouki, A. Koochari; **Writing (original draft)**: A. Ghanbari Talouki, A. Koochari; W**riting (review and editing of the manuscript):** A. Ghanbari Talouki, A. Koochari; **Visualization**: A. Koochari; **Supervision**: A. Koochari; **Project administration**: A. Koochari.

https://orcid.org/0000-0003-0584-6470